LA-4923-PR
A Progress Report
UC-48
ISSUED: April 1972

los alamos
scientific laboratory
of the University of California
LOS ALAMOS, NEW MEXICO 87544

Annual Report of the Biological and Medical Research Group (H-4) of the LASL Health Division

January through December 1971

by

C. R. Richmond
G. L. Voelz

Experimental animals used in work presented in this report were maintained in animal care facilities which are fully accredited by the American Association for Accreditation of Laboratory Animal Care.

TABLE OF CONTENTS

	Page
FOREWORD	6
TABLE OF ORGANIZATION	7
TEMPORARY APPOINTMENTS	8
LOS ALAMOS SCIENTIFIC LABORATORY	10
HEALTH RESEARCH LABORATORY	11
LABORATORY RESOURCES	13
INTRODUCTION	15

THE HOT PARTICLE PROJECT

INTRODUCTION	18
PREPARATION AND PROPERTIES OF MICROSPHERES	18
Preparation of Zirconia Sols	18
Preparation of Microspheres	19
Properties of the Ceramic Microspheres	19
EXPERIMENTAL CONDITIONS	27
Exposure of Animals	27
Sphere Distribution in the Lung	28
Retention and Excretion	30
BIOLOGICAL RESULTS	31
PROSPECT	33

MOLECULAR RADIOBIOLOGY SECTION

INTRODUCTION	35
SYNTHESIS AND RADIOSENSITIVITY OF MODEL DNA	36
Chemical Synthesis	36
Enzymatic Synthesis	38
The Thymine Photodimer	40
X-Irradiation	41
RADIATION AND GENETIC INFORMATION TRANSFER	42
Replication and Amplification	42
Transcription	43
Translation	45
Effects of X-Irradiation upon Transcription	46
EFFECTS OF IONIZING RADIATION ON CHROMATIN STRUCTURE AND THE MITOTIC APPARATUS	47
Effects of Ionizing Radiation on Chromatin Structure and Metabolism	47
Effects of Ionizing Radiation on Components of the Mitotic Apparatus	49

Page

CELLULAR RADIOBIOLOGY SECTION

INTRODUCTION 51

REGULATORY AND CONTROL MECHANISMS IN THE MAMMALIAN CELL CYCLE 52

Low Molecular-Weight RNAs of Post-Ribosomal Particles 52

Effects of Isoleucine Deficiency on Nucleic Acid and Protein Metabolism in Cultured Chinese Hamster Cells 59

Response of Histone Metabolism to X-Irradiation 61

Effects of X-Irradiation on DNA Precursor Metabolism and DNA Replication in Chinese Hamster Cells 64

SURFACE PHENOMENA AND CELLULAR INTERACTION 67

Cell-Cycle Dependent Desquamation of Heparan Sulfate from the Cell Surface 67

CHROMOSOME STRUCTURE AND FUNCTION IN NORMAL, IRRADIATED, AND TRANSFORMED CELLS 70

DNA Constancy in Heteroploidy 70

The Relationship between Heteroploidy and Chromosomal Nondisjunction 74

DNA-Membrane Associations in Cultured Chinese Hamster Cells 76

Repair of Radiation Damage and Replication of a Bacterial Virus Chromosome 76

MAMMALIAN RADIOBIOLOGY SECTION

INTRODUCTION 79

COMPARATIVE RESIDUAL BIOLOGICAL EFFECTS OF RADIATION DOSE PROTRACTION BY FRACTIONATION AND CONTINUOUS GAMMA-RAY EXPOSURE IN DOGS AND MONKEYS 80

Comparative Biological Effects of Low Dose-Rate Exposure in Beagles and Macaca mulatta Monkeys 80

Hematopoietic Response of Monkeys to Fractionated Gamma-Ray Exposures 81

BIOLOGICAL EFFECTS OF RADIATION DOSE PROTRACTON BY FRACTIONATION, CONTINUOUS GAMMA-RAY EXPOSURE, AND CHANGING DOSE RATE IN MICE 82

Comparative Effects of Radiation Dose Protraction by Fractionation and by Continuous Exposure in Mice 82

Effects of Changing (Build-Up and Decay) versus Fixed Dose Rate on Mean Survival Time of Mice 83

MAMMALIAN METABOLISM SECTION

INTRODUCTION 86

MERCURY-203 RETENTION IN RATS 87

ABSORPTION OF SILVER-110 IN RATS 88

SELENIUM-75 DISTRIBUTION IN MICE AFTER CHRONIC EXPOSURE 90

CESIUM-137 ACTIVITY IN A NORMAL NEW MEXICO POPULATION (JANUARY 1970–DECEMBER 1971) 91

BIOPHYSICS SECTION

INTRODUCTION 94

CELL ANALYSIS AND SORTING INSTRUMENTATION DEVELOPMENT 96

An Improved Instrument for Quantitative Cellular Fluorescence Measurements on Single Cells 96

Differential Light Scattering: A Possible Method of Mammalian Cell Identification 100

Multiparameter Cell Analysis and Sorting 104

	Page
BIOLOGICAL APPLICATIONS OF CELL ANALYSIS AND SORTING	107
Life-Cycle Analysis of Cells by Flow Microfluorometry and Labeled DNA Precursors	107
Monitoring Ploidy of Cell-Culture Systems by Flow Microfluorometry	110
Immunofluorescent Measurements with Flow Microfluorometry	113
PHYSICAL RADIOBIOLOGY AND COMPUTER APPLICATIONS	116
In Vivo Measurement of Plutonium Lung Burdens and Lead-210 in the Skull	116

ISOTOPE APPLICATIONS SECTION

INTRODUCTION	119
PREPARATION OF COMPOUNDS LABELED WITH STABLE ISOTOPES	121
Organic Synthesis	121
Biosynthesis	124
STABLE ISOTOPES IN BIOMEDICAL RESEARCH	126
Biochemistry	126
Clinical Applications	128
Effects of High Levels of Carbon-13 Incorporation on Biological Systems	128

ANIMAL COLONY ACTIVITIES

INTRODUCTION	131
Variety of Animals Utilized	131
Disease Surveillance	132
Support Activities	132
Compliance with Federal Laws	133

APPENDIX

1971 BIBLIOGRAPHY FOR BIOMEDICAL RESEARCH GROUP	134
Molecular Radiobiology Section	134
Cellular Radiobiology Section	135
Mammalian Radiobiology Section	136
Mammalian Metabolism Section	137
Biophysics Section	137
Isotope Applications Section	138
Veterinary Section	139
MAJOR SYMPOSIA AND SEMINARS -- 1971	140
TALKS PRESENTED AT SEMINARS AND MEETINGS BY BIOMEDICAL RESEARCH GROUP STAFF	141
Molecular Radiobiology Section	141
Cellular Radiobiology Section	141
Mammalian Radiobiology Section	142
Mammalian Metabolism Section	143
Biophysics Section	143
Isotope Applications Section	144
RESEARCH INTERESTS OF BIOMEDICAL RESEARCH GROUP DIRECTIVE STAFF MEMBERS	145
COMMITTEES ASSOCIATED WITH THE BIOMEDICAL RESEARCH PROGRAM	148

FOREWORD

This report summarizes research activities of the Los Alamos Scientific Laboratory's Biomedical Research Group for calendar year 1971. Because several years have elapsed since the last annual report was published, we have included information on organization of the group, research interests of the staff, and supporting facilities available at the Los Alamos Scientific Laboratory. Although for administrative purposes the group is comprised of seven sections, the technical portion of this report is based upon major areas of research and reflects the multidisciplinary approach to problem solving, which is a basic ingredient of our research philosophy.

The format is akin to that of Science with the goal of transmitting a maximum of information in a concise manner with a minimum of technical detail. Work which has been published or submitted for publication has not been duplicated in this report. A list of publications for 1971, which follows as an appendix, allows the reader to consult the published literature for additional specific technical detail.

BIOMEDICAL RESEARCH GROUP[†]

C. R. Richmond, Ph.D., Group Leader
D. G. Ott, Ph.D., Alternate Group Leader
E. C. Anderson, Ph.D., Assistant Group Leader for Special Problems
O. S. Johnson, B.S., Administrative Deputy
E. M. Sullivan, Administrative Specialist
H. L. Barrington, Clerk-Typist
J. M. Verre, Receptionist-Telephone Operator

CELLULAR RADIOBIOLOGY SECTION

D. F. Petersen, Ph.D., Section Leader

Staff Members

B. J. Barnhart, Ph.D.
E. W. Campbell, B.S.
S. G. Carpenter, B.A.
S. H. Cox, B.A.
M. D. Enger, Ph.D.
L. R. Gurley, Ph.D.
P. M. Kraemer, Ph.D.
P. C. Sanders, M.S.
A. G. Saponara, Ph.D.*
R. A. Tobey, Ph.D.
R. A. Walters, Ph.D.

Postdoctoral Appointees

L. L. Deaven, Ph.D.
C. E. Hildebrand, Ph.D.

Chemistry Technician

J. L. Hanners

Cell Culture Technician

J. G. Valdez

MOLECULAR RADIOBIOLOGY SECTION

F. N. Hayes, Ph.D., Section Leader

Staff Members

J. M. Hardin, M.S.
D. E. Hoard, Ph.D.
A. M. Martinez, B.S.
E. L. Martinez, B.S.
B. J. Noland, B.A.
R. L. Ratliff, Ph.D.
G. R. Shepherd, Ph.D.
D. A. Smith, Ph.D.
D. L. Williams, M.S.

Postdoctoral Appointee

G. F. Strniste, Ph.D.

Chemistry Technicians

V. E. Mitchell
E. C. Wilmoth

BIOPHYSICS SECTION

M. A. Van Dilla, Ph.D., Section Leader

Staff Members

L. S. Cram, Ph.D.
P. N. Dean, M.A.
J. H. Larkins, B.S.
P. F. Mullaney, Ph.D.
J. D. Perrings
A. Romero, B.S.
J. A. Steinkamp, Ph.D.
T. T. Trujillo, B.S.

Postdoctoral Appointee

H. A. Crissman, Ph.D.

Electronics Technicians

M. T. Butler
L. J. Carr
J. L. Horney
W. T. West

AWU Graduate Fellow

A. Brunsting

VETERINARY SECTION

L. M. Holland, D.V.M., Section Leader

Staff Members

P. M. LaBauve, B.A.
J. R. Prine, D.V.M.

Animal Colony Asst. Mgr.

E. A. Vigil

Medical Stenographer

B. B. Gettemy***

Histopathology Technician

R. H. Wood

Animal Technicians

J. E. Atencio
F. Benavidez
J. Cordova**
J. S. Martinez
R. Martinez
E. C. Rivera
L. Salazar
J. B. Sanchez
F. Valdez

MAMMALIAN RADIOBIOLOGY SECTION

J. F. Spalding, Ph.D., Section Leader

Staff Members

M. R. Brooks, B.Ch.E.
O. S. Johnson, B.S.
J. M. Langham, B.S.

Biology Technician

R. F. Archuleta

MAMMALIAN METABOLISM SECTION

J. E. Furchner, Ph.D., Section Leader

Staff Members

G. A. Drake, B.S.
J. E. London, B.S.
J. S. Wilson, B.S.

ISOTOPE APPLICATIONS SECTION

D. G. Ott, Ph.D., Section Leader

Staff Members

C. T. Gregg, Ph.D.
J. Y. Hutson, Ph.D.**
V. N. Kerr, M.A.
V. H. Kollman, M.S.
T. W. Whaley, Ph.D.

Chemistry Technician

T. G. Sanchez

Undergraduate Co-op Students

V. S. Chavez[+]
M. P. Martin

(alternate 6 months at Highlands University; are LASL SCP-4 chemistry technicians)

LIAISON PERSONNEL

J. C. Hensley II, D.V.M., USDA Diagnostic Services, National Animal Disease Laboratory

D. M. Holm, Ph.D., LASL USDA/LASL Liaison for Program Planning

[†] As of January 4, 1972.

* Leave of absence.

** Casual.

*** Half-time.

[+] Now at school.

INTRODUCTION

A significant historical event which altered the course of mankind occurred on February 23, 1941, when Dr. G. T. Seaborg and colleagues discovered the element plutonium in room 301 of Gilman Hall at Berkeley. The isotope of mass-238 and not the more familiar mass-239 was first discovered at that time; the plutonium isotope of mass-239 was not isolated until the spring of 1941, and element 94 remained unnamed until March of the following year. On March 28, 1941, 0.5 μg of plutonium-239 was fissioned by thermal neutrons, and the enormous effort to produce plutonium-239 in quantity for military purposes was begun. The potential toxicity of plutonium was recognized soon after its discovery and availability in quantities for biomedical research.

It is worth recalling that only extremely small quantities of this precious material were available for experimentation during the early 1940's. As an example, the following memorandum written to the Director of the Health Division of the Metallurgical Laboratory is indicative of the early concern about the potential toxicity of plutonium. The memorandum states in part: "It has occurred to me that the physiological hazards of working with plutonium and its compounds may be very great. Due to its alpha radiation and long life it may be that the permanent location in the body of even very small amounts, say 1 milligram or less, may be very harmful. The ingestion of such extraordinarily small amounts as some few tens of micrograms might be unpleasant, if it locates itself in a permanent position. In the handling of the relatively large amounts soon to begin here and at site Y (Los Alamos), there are many conceivable methods by which amounts of this order might be taken in unless the greatest care is exercised. In addition to helping set up measures in handling so as to prevent the occurrence of such accidents, I would like to suggest that a program to trace the course of plutonium in the body be initiated as soon as possible. In my opinion, such a program should have the very highest priority." The writer of this memorandum was Dr. Glenn T. Seaborg, and the date was January 1944.

The biomedical research program at Los Alamos has evolved from its conception in 1943 as a small Health Group established to protect the health of the workers, to develop safe working procedures, and to establish tolerance levels for exposure to radioactivity, plutonium, and other radionuclides. In 1944, once significant amounts of plutonium began to accumulate at Los Alamos, the Laboratory Director, Dr. J. Robert Oppenheimer, at the request of the Health Group, authorized the temporary establishment of a group of four people to initiate a research program designed to develop tests for setting exposure limits for plutonium. Several months later, this small group was absorbed by the Health Group as a Biochemistry Section, and the Laboratory's biomedical research program was born. In 1945, the Section moved into a small building of its own, and its members established the urine assay procedure for diagnosing exposure of Laboratory personnel to plutonium. Experiments were conducted which led to the first successful labeling of a biologically-important compound (nicotinic acid) with reactor-produced carbon-14. The first measurement of carbon-14 by scintillation counting procedures was accomplished here and formed the basis for the present generation of commercially-available liquid scintillation counting systems.

By 1948, the Health Group was a Division in the Laboratory, and the Biochemistry Section became Group H-4, the Biomedical Research Group. In October 1952, the group moved from temporary wooden structures (Fig. 1) into its present building and by the end of that decade had established itself in both national and international circles as an authority on the effects of radiation from nuclear weapons, worldwide fallout, and the physiology and toxicology of tritium and plutonium.

Fig. 1. Makeshift building used for biomedical research activities during the war years (photographed in 1946 showing three additions to the original structure).

The Biomedical Research Group pioneered in and became a recognized authority on liquid scintillation counting, synthesis of isotopically-labeled organic compounds, use of radioactive tracers in biology and medicine, and whole-body counting techniques and applications to biomedical research. By utilizing the development of large-volume liquid scintillation detectors, the group contributed significantly to the field of anthropometry through its capability to measure total-body potassium by quantitating the natural level of potassium-40 within the human body. By exploiting the whole-body counting systems designed for both research animals and man and making use of the Laboratory's significant computer capabilities, the Biomedical Research Group contributed significantly to the field of radiation protection by conducting studies on the uptake, distribution, and excretion of radioisotopes by animals and man. The interest in metabolic kinetics was also applied to the emerging field of nuclear medicine during the late 1950's.

Shortly after the discovery in 1955 of the presence of cesium-137 in man from worldwide nuclear fallout, measurements were begun on a controlled population of subjects residing in the Los Alamos area. These studies have continued to the present time and represent perhaps the most meaningful documentation of the temporal changes in man of a radioactive material released to the environment.

Beginning in the early 1960's, more emphasis was placed on the fundamental research aspects of the biomedical research program. Although investigations continued in the Mammalian Metabolism and Mammalian Radiobiology Sections related to the response of higher organisms to ionizing radiations and radioactive materials, a major emphasis was directed toward research in the fields of molecular and cellular biology.

The late 1960's also marked the start of a research program related to the question of the probable biological effects resulting from non-uniform dose distribution of alpha-emitting particulates in the lung. Interestingly, this very difficult problem has received considerable attention but little resolution since the mid-1940's. This particular problem is now one of the highest priority because of the vast potential applications of the element plutonium as regards breeder reactors, space nuclear power systems (radioisotopic thermoelectric generators), medical applications such as the heart pacer and artificial heart, as well as production, transportation, and deployment of this material for national defense. It is interesting in a sense that part of the group is now actively working on the problem which relates to plutonium efforts conducted some 20 years previously at LASL.

The 1970's have witnessed the emergence of an interest in the stable isotope program designed to exploit the use of stable elements in the general field of biomedical research. In 1971, an Isotope Applications Section was formed within the group to concentrate on the biomedical aspects of the ICONS (Isotopes of Carbon, Oxygen, Nitrogen, and Sulfur) program which involves several groups within the Los Alamos Scientific Laboratory.

The Molecular Radiobiology Section is engaged in a variety of organic synthesis procedures to assemble polynucleotides having known base sequences. Certain enzymes that catalyze polynucleotide synthesis are not only being isolated and purified but are also being studied as biofunctional proteins participating in information transfer reactions. The structure, function, and metabolism of both acidic and basic nuclear proteins, believed to be involved in readout of genetic specifications and thus differentiation, are being investigated.

Biologists and biochemists in the Cellular Radiobiology Section are investigating the temporal sequence of a variety of cellular processes in relation to specific phases of the cell life cycle using synchronized cultures of mammalian cells. A method has been developed in this Laboratory for producing relatively large quantities of cultured mammalian cells synchronized with respect to period in the life cycle. Using these cultures mechanisms controlling synthetic processes, energy metabolism, recovery from ionizing radiation, cell-surface phenomena, and mathematical methods of cell growth are being investigated. Several members of the Molecular Radiobiology Section are using synchronized cultures to examine the synthesis, turnover, and structural alterations of nuclear and cytoplasmic basic proteins. In addition to studies on animal

cells, investigations are in progress on survival of microorganisms exposed to ultraviolet and ionizing radiations and the biochemistry of bacterial genetic transformation.

The Biophysics Section is mainly concerned with development and improvement of instrumentation for cell biology research. In collaboration with the Cellular Radiobiology Section, electronic instruments have been developed for high-apeed electronic cell counting and cell sizing. A high-speed sorter has been invented which can physically separate living cells in suspension according to cell volume. A fluorescent cell spectrometer has been developed which utilizes a laser to provide the high intensity and collimation of the light of excitation required to determine rapidly and quantitatively the DNA content of the individual cells of a cell population. Both cell sensing and sorting efforts are currently being extended to other optical and multiparameter methods. The Biophysics Section also provides general electronics, mechanical engineering, radiological physics, and computer science support for the group.

THE HOT PARTICLE PROJECT

INTRODUCTION

The objective of the Hot Particle Project is to study possible carcinogenesis and other hazards resulting from localized irradiation of tissue by highly radioactive, insoluble microparticles with emphasis on PuO_2 in the lung. We will attempt to relate experimental tumor incidence to two functions: (1) the number of cells receiving a given dose, and (2) the probability that a cell receiving a dose gives rise to a tumor. The quantitative prediction of tumor incidence per sphere is then the product of the two functions integrated over all cells in the radiation field of the sphere. The first function, the distribution of dose, can be established by Monte Carlo averaging over representative sections of the lung. The second, the dose-response function, is accessible in principle by direct measurement of the effects of uniform doses, but accurate extrapolation to other organs and/or animals requires a mathematical model based on fundamental mechanisms taking into account the pertinent dynamics of malignant transformation, stem cell progression, immunological reactions, and such cooperative effects as influence development of the tumor. Therefore, our program is two-fold: (1) measurement of tumor incidence in experimental animals, and (2) development of mathematical models.

The animal chosen for the principal experiment is the golden (or Syrian) hamster. Primary reasons for the choice were freedom from general respiratory problems and the extensive use of this animal in experiments with other tumorigenic agents. To facilitate the calculations of dose distribution and measurement of the effect of particle specific activity, maximum uniformity has been required of the particles, and immobility is desirable. To achieve these ends, the requisite amount of alpha radioactivity is incorporated into ceramic microspheres of ZrO_2 of such diameter (10 μm) that they will lodge in the capillary bed of lung alveoli following jugular injection. Serial sacrifice of the hamsters over their normal life span will provide material for histological and pathological evaluation of biological damage and for the measurement of distribution and retention of the microspheres. The biological results will be correlated with the predictions of mathematical models to be further developed along lines already indicated (1-3) but with increasing biological sophistication and inclusion of more detailed mechanisms.

The project began early in 1970, and the first year was spent largely in preparing animal quarters, developing care and quarantine procedures, and in exploring methods of microsphere preparation and assay. During the past year, we have made four primary accomplishments: (1) preparation and characterization of the ZrO_2-PuO_2 microspheres used as experimental sources; (2) injection of hamsters at all dose levels of the preliminary experiment, (3) determination of the distribution of spherea within the lungs; and (4) observation of the first biological response to the spheres.

PREPARATION AND PROPERTIES OF MICROSPHERES

Preparation of Zirconia Sols (J. D. Perrings)

The properties of the ZrO_2 sol are very important for proper sphere formation, gelation, and sintering to an insoluble ceramic. Low iron content, absence of chloride, and proper acidity are crucial. The starting material used was zirconyl chloride (Fisher's certified grade). This was converted to nitrate by displacement with concentrated HNO_3 by boiling nearly to dryness three times in a three-necked, round-bottomed flask heated with a Glascol mantle. $AgNO_3$ (0.1 molar) was used as an indicator for the presence of chloride. The zirconyl nitrate so prepared was dissolved in distilled water and dried in a rotary evsporator,

heating the solution in a water bath, and chilling the receiving flask with Dry Ice and alcohol. The purpose of this step is to remove excess HNO_3.

The resulting $ZrONO_3$ (50 g) is then heated for 1 hour at 200°C for further denitrification. The product is dissolved in 200 ml water and polymerized at 28 PSIG in a steam-heated sterilizing autoclave. This material is dialyzed against distilled water in a Visking casing until the pH reaches 2.0. The resultant sol shows a very slight Tyndal effect. The concentration as ZrO_2 is 83.4 g/l. An alternate method of sol denitrification, extraction with 0.1-m Amberlite LA in dodecane, resulted in a sol with a ZrO_2 concentration of 28.8 g/l.

Just prior to sphere generation, the requisite amount of plutonium in the form of $Pu(NO_3)_4$ in 2 N HNO_3 is added to the sol. Either plutonium-238 or plutonium-239 is used, and the total amount is small enough (less than 0.2 ml in 40 ml sol; less than 1 percent PuO_2-ZrO_2) to be without effect on the gelation and sintering of the ZrO_2. Low levels of cobalt-57 are added to some batches to provide a gamma-ray tag.

Preparation of Microspheres (E. C. Anderson and J. D. Perrings)

Microspheres are prepared by a modification of the sol-gel process developed by the Oak Ridge National Laboratory and others for fuel elements (4). Very uniform particles are obtained by using equipment described in detail by Fulwyler (5,6). A 40-μm diameter stream of aqueous ZrO_2 sol is injected into a 1-mm stream of 2-ethyl hexanol in coaxial laminar flow. The 2-ethyl hexanol contains 0.1 percent NH_4OH and 0.05 percent Triton X-100, a surfactant. The sphere size is determined by sol concentration, pressure differential between sheath and core streams, and frequency of the sonic oscillator controlling the rate of droplet formation. Typically, to prepare 10-μm ceramic spheres, the following conditions were used: sol concentration 5.34 g/l., sheath pressure 34 PSIG, core pressure 55 PSIG, oscillator frequency 22 kH.

Approximately 8×10^7 droplets are produced in about 1 hour running time from 40 ml of sol. They are collected in 6 l. of 2-ethyl hexanol and, after 2 hours dehydration time with constant, gentle stirring, the gelled microspheres are collected on a 47-mm diameter, 14-μm pore nylon Millipore filter. They are then washed repeatedly with heptane to remove 2-ethyl hexanol and, after brief drying, are transferred to a 50-ml centrifuge cone and suspended three times in absolute methanol. The product is transferred to an alpha-alumina crucible and dried overnight at 200°C. Firing is started at 200°C and increased to 1000°C by 200°-increments at hourly intervals. Final temperature is maintained for 2 to 3 hours. The spheres undergo the following size transformations in the process: freshly gelled 29- to 30-μm diameter; hepane-washed 21- to 22-μm diameter; methanol-washed 18- to 19-μm diameter; fired 10-μm diameter.

Properties of the Ceramic Microspheres (E. C. Anderson, P. N. Dean, and J. D. Perrings with assistance from S. G. Carpenter, J. Langham, and P. C. Sanders)

The physical properties of the spheres were measured in some detail, both to provide input data for dosimetric calculations and in order to understand the spheres themselves and to improve quality control. The parameters of importance for the biological experiment are the sphere diameter, which determines the trapping in the lung capillary bed, and the alpha specific activity and energy spectrum, which determine the dosimetry. The additional parameters which have been determined are sphere mass and density and the radial distribution of plutonium within the sphere.

Diameter and Volume.--Sphere diameter (nominally 10 μm) can be determined directly by optical microscopy of individual spheres to a precision of a few percent. Somewhat better results are obtained from measurement of the lattices which the spheres often form when a suspending solvent evaporates from a monolayer (Fig. 1). The spheres are then hexagonally close-packed to a high degree of accuracy, and measurements can be made over as many as 20 sphere diameters with attendant reduction in optical errors of boundary identification. Repeated measurements under these conditions show

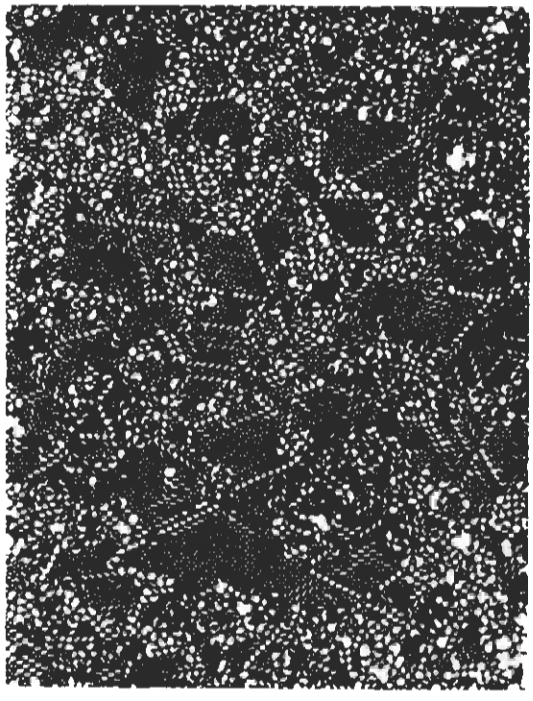

Fig. 1. Photomicrograph of hexagonal lattices formed by microsphere monolayer plated on a slide.

coefficients of variation of less than 1 percent on measurement of average sphere diameter, corresponding to a 3 percent error in calculated volume. The average diameters of the spheres range from 9.90 to 10.87 μm over the 11 batches produced. The mean is 10.28 with a coefficient of variation (C. V.) of 3.2 percent among batches and corresponds to a mean volume of 571 μm^3.

The precision of the determination of diameter of individual spheres is not good enough to define the volume variability among spheres of the same production batch. Measurements of the distribution of sphere volumes with a Coulter spectrometer give a C. V. of 4 percent (1.3 percent on diameter), of which a significant fraction is thought to be due to instrumental resolution. Volume variability is presumably less than variability of plutonium content, which was measured as less than 2.6 percent (see section on Plutonium Content of Microspheres, below).

Mass of Individual Spheres.--In principle, the average mass per sphere can be calculated from the total mass (volume x concentration) of ZrO_2 passed through the droplet generator and the number of drops generated (frequency of oscillator x running time). Because of the stability of the system and the observed uniformity of sphere volumes, the calculation should be reliable. While a direct independent verification of the mass has not been made (the mass of a single sphere is about 2.8 x 10^{-9} g), the principle of the calculation can be checked by comparing a similarly calculated plutonium content with the measured value. These results (see section on Plutonium Content of Microspheres, below) suggest that the mass calculation is accurate. The calculated average mass ranges from 2.62 to 2.98 ng for the 11 batches, with a mean of 2.80 ng and a C. V. of 4.3 percent among batches.

Densities of Spheres.--From the volumes and masses arrived at above, one can calculate the average density for the spheres of each batch. The rather surprising results are summarized in Fig. 2, which is a plot of mass versus volume with the solid lines representing loci of equal densities. The densities range from 4.25 to 5.60, but only three discrete densities are found: 5.55 ± 0.06, 5.00 ± 0.06, and 4.29 ± 0.05. The highest density corresponds to that expected for crystalline ZrO_2; the lower ones presumably represent material which has failed to sinter completely and which still

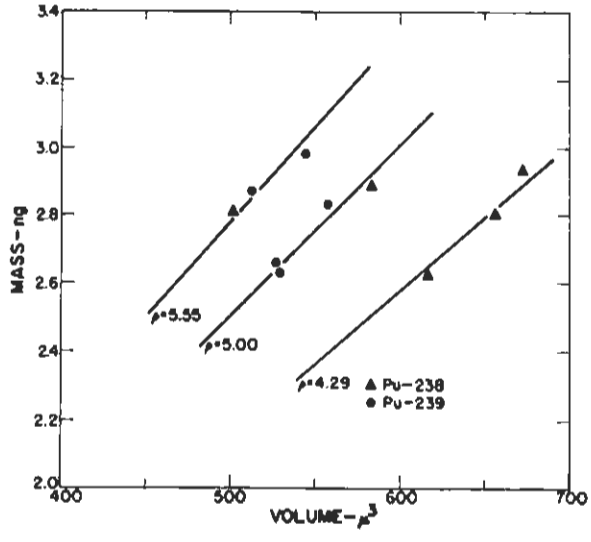

Fig. 2. Mass, volume, and densities of ZrO_2-PuO_2 microspheres.

contains voids. No reason is known for the discrete grouping. It does not correlate with PuO_2 content nor with the use of plutonium-238 rather than plutonium-239. There is a partial correlation of density with age of the ZrO_2 sol; the last three batches are all of the lowest density. However, the highest density spheres were preparation Nos. 3, 4, 5, and 7. Thus, aging of the sol (increase in micelle size?) might account for the lowest density but not for the other two groups. One of the groups of lowest density was refired an additional 20 hours at 1000°C (normal firing time 2 hours), but the density increase (about 4 percent) was small compared with the separation between density groups.

It is possible to demonstrate by an independent measurement that the density differences are real. The energy lost by an alpha particle traversing matter is proportional to the mass per unit area along its track. This quantity is the product of path-length x density. The measured energy distribution spectrum of alpha particles from a monolayer of spheres in well collimated geometry has a sharp cutoff at a minimum energy corresponding to the maximum path-length through the sphere (i.e., the diameter). In Fig. 3 we plot ρd, the product of sphere density x diameter in $pg/\mu m^2$ against the observed maximum energy loss in MeV. An excellent linear correlation is obtained, confirming the reality of density variation. The product ρd (which is proportional to mass ÷ diameter^2) has a C. V. of 7.3 percent (due to mass variability of C. V. = 4 percent combined with an essentially uncorrelated d^2 variability of 6 percent). The energy loss also has a C. V. of 7.3 percent. The calculated absorption coefficient (ΔE/ρd), on the other hand, has a C. V. of only 1 percent. (For a more rigorous analysis of the stopping power of the spheres, see the section on Radiation Distribution of Plutonium within Spheres, below).

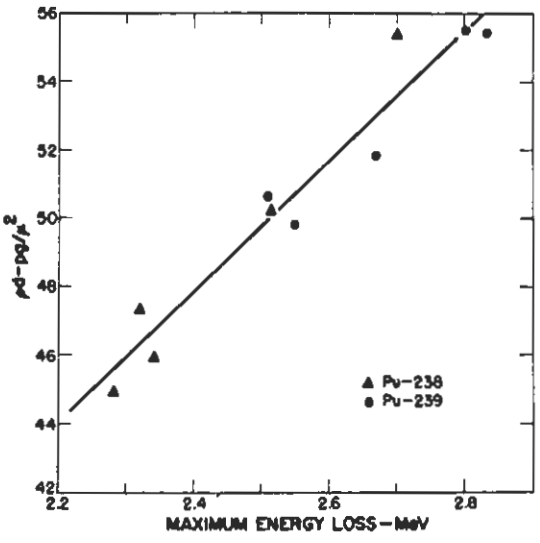

Fig. 3. Relation between mass/area and maximum alpha energy loss for the microspheres (10 $pg/\mu m^2$ = 1 mg/cm^2).

Plutonium Content of Microspheres.--Total alpha counting rate is determined by an internal-sample, gas proportional counter using a few thousand spheres per sample. The spheres are plated on a specially made graticle about 8 mm square, ruled with a 250-μm grid, which permits very accurate visual scoring of sphere number. The results of this direct determination of average specific activity can be compared with the value calculated from the known amount of plutonium added to the ZrO_2 sol and the number of spheres generated. Such a comparison is made in Fig. 4 for the 1000-fold range of concentration covered (see following page). The solid line is drawn with a 45° slope and corresponds to a constant counter efficiency of 48.3 percent, the average ratio of measured rate to calculated. The C. V. of the ratio found/taken is 4 percent with the two lowest points omitted. These results confirm the quantitative retention of plutonium in the spheres and also confirm the reliability of the calculation of total number of spheres produced per run and, hence, of the mass calculated in the section on Mass of Individual Spheres (above). A similar method is used to determine the cobalt-57 specific activity by counting the graticle of spheres in 4π geometry between two 3 x 3-in. NaI (Tl) crystals. The average level of cobalt-57 is 0.5 pCi per sphere. The plutonium activity ranges from 0.07 to 59 pCi per sphere (10 to 7900 alphas per hour per sphere), corresponding in activity to

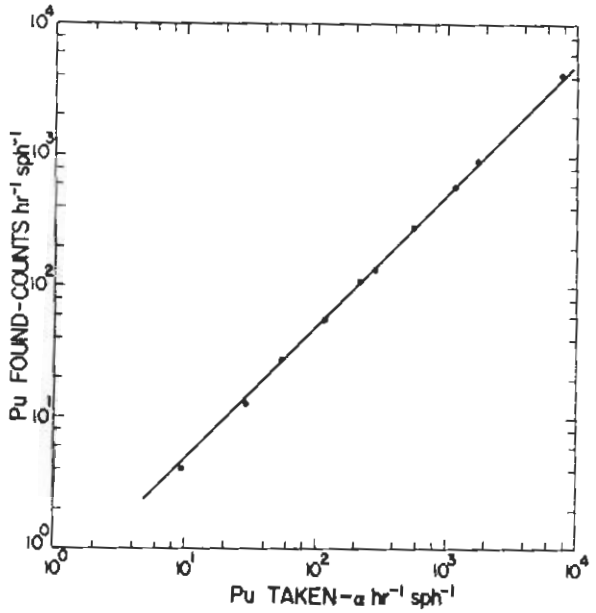

Fig. 4. Comparison of measured specific activity of microspheres with that expected.

pure $^{238}PuO_2$ spheres with diameters from 0.09 to 0.86 μm. The lower levels were prepared with plutonium-239 and the upper with plutonium-238 so that the weight fraction of PuO_2 in the ZrO_2 varied only from 3×10^{-5} to 1×10^{-2}.

Measurement of the variability of plutonium concentration among spheres of a given batch was possible only at the highest concentrations. (Alpha autography, the only counting method with enough sensitivity for measuring individual spheres at the lower levels, is not sufficiently precise.) By placing single, high-level spheres in a sandwich between ZnS-coated plastic circles, it was possible to obtain good statistical counting precision in reasonable counting times. For single spheres of Batch Zr33 (Level 6), a C. V. of 3.3 percent was measured of which 2.1 percent was ascribable to counting statistics, leaving an excess of 2.6 percent from variability in plutonium concentration plus variability due to other random measment errors (such as variation in counting geometry). This C. V. is less than the 4 percent variability of sphere volume estimated as an upper limit by Coulter volume spectrometry.

No biological effects are expected from the temperature of spheres of this low a specific activity. From the rate of energy release and a coefficient of thermal conductivity, a temperature gradient of 8×10^{-9}° /μm is calculated for a sphere immersed in an organic liquid and 4×10^{-8}° /μm in air. Convective transport of heat, of course, will make the gradient even lower. Therefore, the spheres must be within a very small fraction of a degree of the temperature of tissue.

Radial Distribution of Plutonium within Spheres.--For the purposes of dosimetry, it is not usually necessary to know the plutonium radial distribution; the emergent alpha-energy spectrum is adequate. However, for an exact calculation the radial distribution is relevant as it determines the angular distribution of the alpha flux with respect to sphere surface. This factor may be significant for precise dosimetry close to the sphere. The plutonium distribution is also of interest in connection with quality control and for a better understanding of the mechanisms of sol gelation and sphere sintering.

Because of the uniform initial energy of the plutonium alpha particles (within the resolution of these measurements) and the unique correspondence between energy loss and path-length in an absorber, the energy spectrum of alphas emerging from a sphere is simply related to the distribution of path-lengths traversed within the sphere. The latter distribution is related, although less simply, to the radial distribution of plutonium. The following solution is due to G. I. Bell, LASL Theoretical Division.

A typical energy spectrum is shown in Fig. 5 (see following page). (The low-energy tail, amplification X 10, is the result of poor response at the edge of the silicon surface-barrier layer detector.) Measurements are made in a vacuum spectrometer with the 20-mm diameter detector at a distance of 240 mm from a monolayer of spheres to collimate the counting geometry. The relation between energy and path-length is obtained by assuming that the rate of energy loss (the stopping-power, dE/dx) is a power function of E:

$$dE/dx = -k E^{-\alpha} \qquad \text{(Eq. 1)}$$

Integrating over a path-length $x = \ell$, corresponding

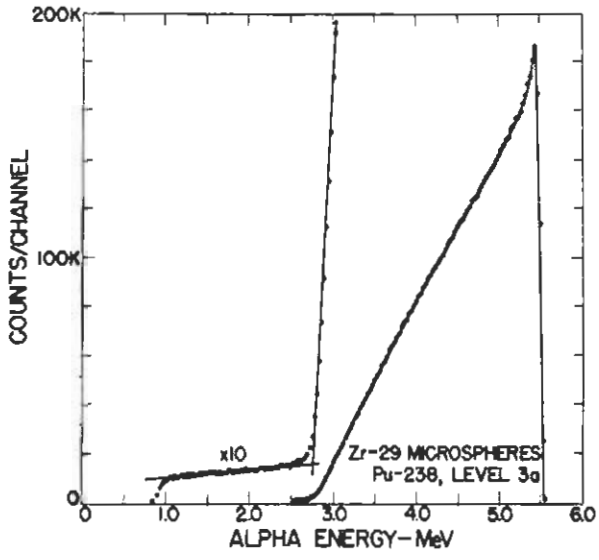

Fig. 5. Typical alpha energy spectrum of microspheres measured in vacuum spectrometer with a silicon surface-barrier detector.

to an energy loss from E_o to $E(\ell)$, and solving for ℓ gives

$$\ell = \frac{1}{k(\alpha + 1)} \left[E_o^{\alpha + 1} - E(\ell)^{\alpha + 1} \right] \qquad \text{(Eq. 2)}$$

Determination of the values of k and α are discussed below. Equation 2 is used for the numerical conversion of measured energy spectrum (a histogram) to the corresponding distribution of path-lengths.

The physical basis of the calculation of radial plutonium distribution is illustrated in Fig. 6. Consider those alphas having path-lengths in the sphere ranging from 0 to ε. Assuming the detector to be at a distance large compared with its diameter, all paths in the sphere which reach the detector are nearly parallel to the sphere-detector axis. Therefore, the locus of all points in the sphere giving paths of length 0 to ε is the space bounded by the upper surface of the sphere and another surface of the same radius R whose center is shifted downwards a distance ε along the sphere-detector axis. The upper shaded area represents the section of this volume in the plane of the figure. The volume is a sample of the spherical shell between R and R - ε, but it is a non-representative sample. However, if ε is taken small

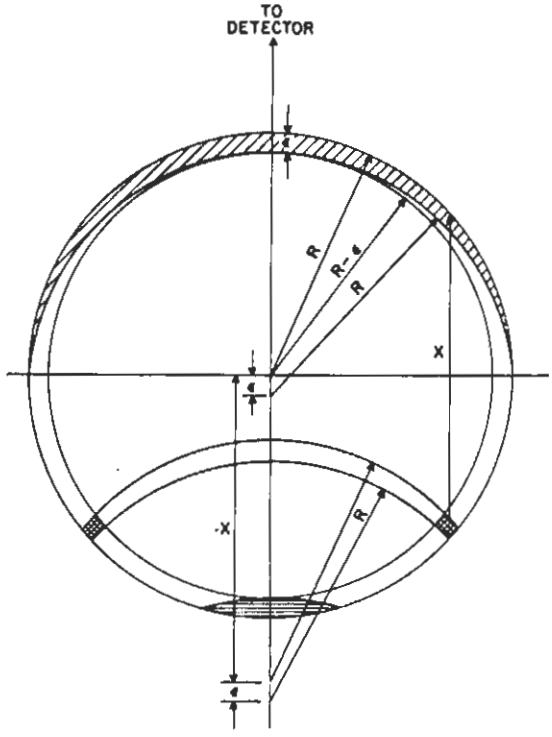

Fig. 6. Cross section of microsphere to illustrate geometrical factors in the relation between volume elements and path-lengths in the sphere.

enough so that the plutonium concentration does not vary significantly over this distance, then an average value of that concentration for the shell can be calculated from the path-length spectrum area between $\ell = 0$ and $\ell = \varepsilon$. In practice, this requires very precise data with high energy resolution and/or smoothing the data with a high-order polynomial.

This outermost shell of the sphere will also make contributions to the rest of the path-length spectrum. Thus, for any path-length $0 \leq X \leq 2R$, there is a corresponding volume in the outer shell. This volume is bounded by the shell and by two spheres of radius R whose centers are displaced downwards by distances X and X + ε, respectively, as indicated in the figure. Calculation of the volume in the shell associated with path-length X is purely geometric. Thus, one can calculate the entire path-length spectrum due to the outermost shell of the sphere and subtract it from the measured spectrum. The residual spectrum will be due to a smaller sphere of radius R - ε. The calculation can be iterated, stripping away successive

shells and generating the complete radial distribution of plutonium.

In practice, several difficulties have been encountered. Clearly, as the stripping proceeds, errors will accumulate and the calculated concentration will become less accurate. This problem is mitigated by the fact that the center of the sphere corresponds to path-length R, whereas the entire spectrum extends to path-length 2R. Only the upper half of the spectrum is required to give the complete radial distribution, and the lower half can be used for an independent calculation or for a check of the appropriateness of the assumed values of k and α in the dE/dx law.

A more serious and fundamental difficulty is the numerical instability of the solution, which results from the inherent "ill-posed" nature of the problem. W. L. Hendry (LASL Theoretical Division) has shown that the problem (7) is equivalent to the solution of a Volterra integral equation of the first kind and has developed least-squares methods of solution which stabilize the calculation. The stripping and Volterra methods give identical results for the outer portions of the sphere; unless physically reasonable constraints are placed on the solutions, both diverge for the central regions of the sphere, which contain only a negligible (less than 1 percent) fraction of the total sphere volume.

The value of α in Equations 1 and 2 is expected to be 0.4 on the basis of the slope of Northcliffe's summary graph (page 88 of Ref. 8) over the range 2 to 6 MeV for alphas. Proof of this value is provided by Fig. 7, which is a plot of the fractional residual error in calculation of the lower half of the plutonium alpha spectrum from the radial concentration determined by the upper half of the same spectrum. The calculation was performed assuming values of α of 0.2, 0.4, and 0.6. The fit for 0.4 is very good, the residual error being less than 5 percent everywhere. In addition to confirming the choice of α, this result also adds confidence to the overall method of calculation.

The other constant, k, is determined by solving Equation 2 using the known diameter of the sphere and observed maximum energy loss. (The calculation is actually made for k as a mass absorption

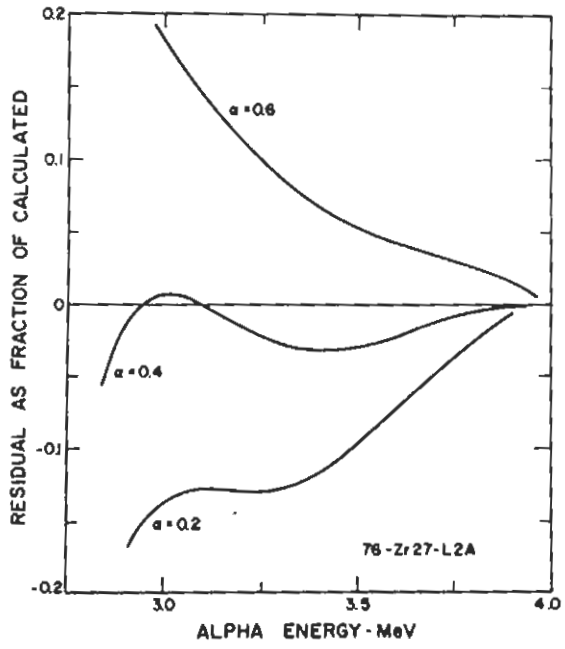

Fig. 7. Effect of choice of α on the quality of fit (see text).

coefficient rather than as a linear coefficient in order to allow for varying densities in different batches. Uniform density is assumed throughout the aphere.) Values of k calculated for the 10 batches have a C. V. of 1.6 percent, and the mean value for plutonium-238 is within 0.4 percent of that for plutonium-239, a significant test in view of different alpha energies. The absolute value calculated for the stopping-power of ZrO_2 at 4 MeV using k = 0.865 and α = 0.4 is 497 keV/mg/cm^2, compared with 521 calculated from the two-variable stopping-power table (page 127, Ref. 9) using values of I_{adj} from Turner's graph (page 100, Ref. 9). The agreement to within 5 percent corresponds to a 2.5 percent absolute error in sphere diameter and is within our estimated experimental errors.

The results for plutonium concentration as a function of sphere radius are shown in Figs. 8 and 9 (see following page). (Concentration at the surface of the sphere is taken as unity.) With the exception of Level 1 (cf. Table 2), the batch with the lowest plutonium activity (but not the lowest chemical concentration), the results are all comparable, showing a concentration maximal at or near the surface and declining to 50 to 70 percent

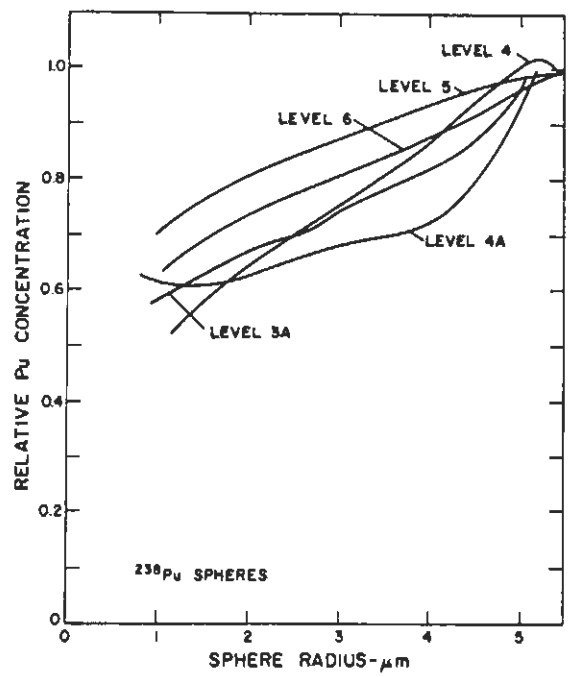

Fig. 8. Radial distribution of plutonium in the plutonium-239 microspheres (for identification of the levels, see Table 2).

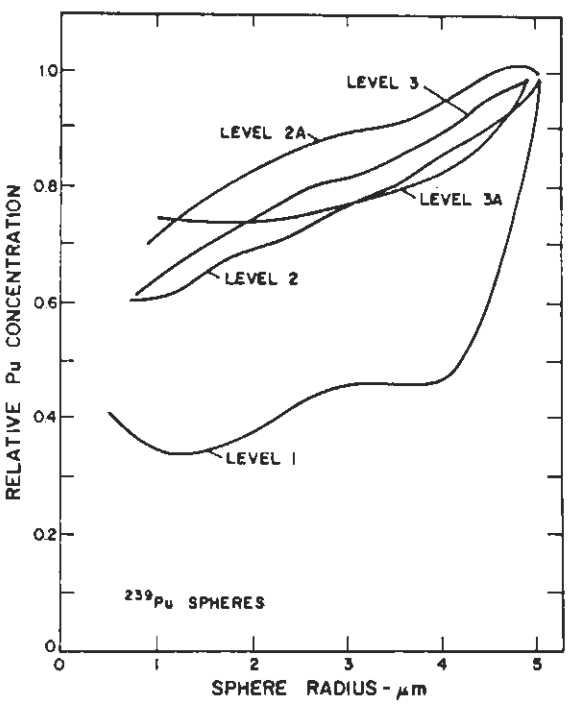

Fig. 9. Radial distribution of plutonium in the plutonium-238 microspheres (for identification of the levels, see Table 2).

towards the center. (We have no explanation for the larger variation of Level 1.) Neither method of mathematical analysis of the data gives a unique answer for the central concentration; physical reasoning suggests that d[Pu]/dr may be zero at the center, therefore, all the curves probably level out at something like their minimal values in the figures. (Note that less than 1 percent of the sphere volume lies within 1 μm of the center.) The reproducibility of repeated analyses of a given batch of spheres suggests a precision of several percent. The differences between batches, therefore, are probably real, but the possibility of systematic errors of 5 percent or more cannot be eliminated at present. The fine structure of the concentrations curve is not necessarily real, since it is influenced by the 10th-degree polynomial smoothing used in both methods of calculation. However, it should be noted that the input data have a very high statistical precision (C. V. about 0.3 percent in the majority of the channels) and resolution (30 keV equivalent to 0.1 μm) and that they have statistically significant structure. The best indication of the overall reliability of the method is the very small values of the residuals shown previously in Fig. 7.

A plutonium concentration declining inward is perhaps not unreasonable in view of the mechanism of the sol-gel-ceramic transformation which occurs during sphere production, drying, and firing. The initial diameter of the droplets generated is about 30 μm, shrinking to 20 μm during gelation and to 10 μm on firing. The relative volumes are of the order of 27:8:1, therefore, there is a large flux of water out of the spheres. The concentration of water will thus be reduced near the droplet surface, and the concentration of plutonium and ZrO_2 will rise. Unless inward diffusion down their concentration gradients is rapid enough to compete with water flux, both may be concentrated near the surface. One might expect the ionic plutonium to be more mobile than the colloidal ZrO_2, but this would lead to an increased plutonium concentration relative to ZrO_2 at the center, contrary to observation. A more important factor may be the precipitation of plutonium as the pH of the droplet is reduced near the surface. Initially, 2 N in HNO_3, the droplet is both dehydrated and neutralized by

the 2-ethyl hexanol-ammonia. Under these conditions, greater mobility of the dissolved plutonium could lead to an enrichment of the Pu/ZrO_2 ratio in the outer regions of the droplet where plutonium is being precipitated onto the ZrO_2 micelles. An important question suggested by this reasoning is the concentration of ZrO_2 within the sphere. Complete recrystallization in the firing process should lead to uniform density as assumed in the analysis of plutonium distribution. If this is not so, then there is an error (probably small) in calculated plutonium concentrations due to an erroneous energy-path length conversion. (The path-length is in $pg/\mu m^2$, but the geometric volume elements in Fig. 6 are in μm^3 and a constant density was assumed in the conversion.) To shed more light on this question, attempts have been initiated to study the microstructure of the ZrO_2 by scanning electron microscopy. The results may illuminate the processes of sphere formation but should not significantly affect the dosimetry.

Cobalt-57 Tag.--In order to facilitate measurement of injected dose and retention, a low-level tag of cobalt-57 has been added to all batches of spheres. Cobalt-57 decays by pure electron capture to a 136-keV excited state. Almost all the energy is emitted as 122 keV (85 percent) and 136 keV (11 percent) gamma rays. Conversion electrons from the 122-keV gamma are of low abundance (4 percent). The 14-keV level is highly converted, but these soft electrons will not escape from the ZrO_2. Thus, for dosimetric putposes, one need consider only the energetic gammas. Only 3 percent of their energy will be absorbed within the body of the hamster. The specific activity of cobalt-57 in the spheres is 60 gammas/hour/sphere and corresponds to a whole-body radiation dose of about 1.3 mR/yr, which is of the order of 1 percent of natural background. So small a dose can probably be considered completely negligible in this experiment. However, control animals with cobalt-57 spheres are being carried along with non-active ZrO_2 controls.

Tables 1 and 2 summarize the properties of the microspheres used in these experiments. Table 1 gives the physical properties of diameter, volume, mass, and density, while Table 2 gives their plutonium content.

TABLE 1. PHYSICAL PROPERTIES OF MICROSPHERES

Parameter	Average	Range among Batches	Coefficient of Variation Intra-batch (percent)	Coefficient of Variation Inter-batch (percent)
Diameter	10.28 μm	9.9–10.9 μm	< 1	3.2
Volume	571 μm^3	502–673 μm^3	< 4	10
Mass	2.80 ng	2.62–2.98 ng	?	4.3
Density	5.55 5.00 4.29	4.25–5.60	?	1.06 1.14 1.05

TABLE 2. PLUTONIUM CONTENT OF MICROSPHERES

Isotope	Level	Batch No.	Specific Activity pCi/sphere	Specific Activity α/min/sphere	Equivalent Diameter Pure $^{238}PuO_2$ (μm)	PuO_2 Weight Fraction
^{239}Pu	1	Zr24	0.07	0.16	0.09	4.3×10^{-4}
	2	Zr25	0.22	0.49	0.13	1.4×10^{-3}
	2A	Zr27	0.42	0.92	0.16	2.9×10^{-3}
	3	Zr22	0.91	2.0	0.21	5.8×10^{-3}
	3A	Zr28	1.6	3.6	0.26	1.1×10^{-2}
^{238}Pu	3A	Zr29	2.1	4.7	0.28	4.8×10^{-5}
	4	Zr31	4.3	9.5	0.36	1.0×10^{-4}
	4A	Zr30	8.9	19.5	0.46	2.0×10^{-4}
	5	Zr32	13.3	29.3	0.52	3.3×10^{-4}
	6	Zr33	59.4	131.0	0.86	1.3×10^{-3}

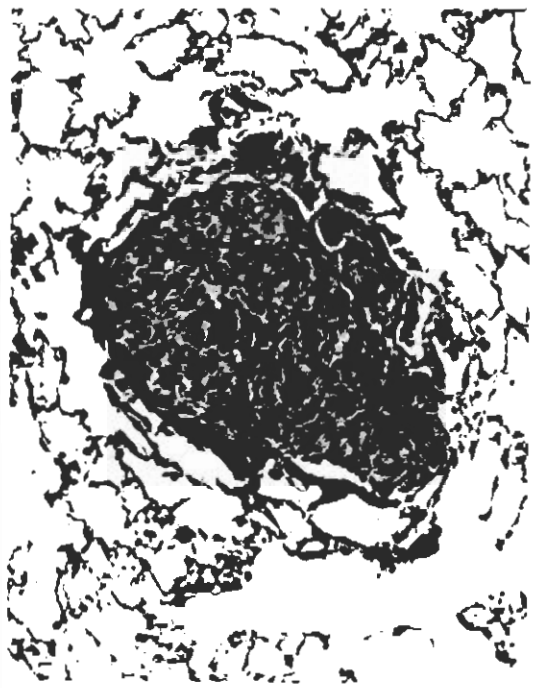

Fig. 16. Four-month exposure at Level 6 showing foreign-body granuloma.

Fig. 17. Four-month exposure at Level 5.

microspheres are found in the same lung with little apparent biological response. In Level 5, which has a 4-fold lower radioactivity, the group with 4 months exposure shows a response similar to that at 1 month in Level 6 (Fig. 17).

Because the only biological response observed thus far is found in the high-activity groups, the indication is that the ZrO_2 microspheres are chemically inert and that the phagocytic and granulomatous responses result from a reaction to dead or dying cells around the microspheres proportional to the cumulated radiation dose. Animals sacrificed from the control group injected with nonradioactive ZrO_2 spheres have yet to exhibit any biological recognition of the presence of the spheres.

PROSPECT

During the coming year, the primary objectives are:

(1) To continue the injection program with hamsters to increase the number of animals committed, especially at the more significant dose levels. Details of activity level, sphere number, and number of animals will depend in part on forthcoming experimental results indicating the areas of interest, such as evidence of over- and underexposure and of the magnitude of tumor probability.

(2) To obtain more detailed information on the developing responses of the lung to the particles, including histological and pathological characterization, quantitative measures of relations to particle number and position, to dose rate and accumulated dose, and to portion of the lung irradiated.

(3) To develop additional experimental protocols to obtain more information about the mechanisms of the genesis and development of tumors (e.g., the role of the immunological system).

(4) To study structural parameters of hamster lung and their effect on alpha range and dose distribution, including experimental measurements on lung sections and computer modeling.

REFERENCES

(1) P. N. Dean and W. H. Langham, Tumorigenicity of Small Highly Radioactive Particles, Health Phys. 16:79-84 (1969).

(2) L. J. Perez, Jr., and J. R. Coleman, A Comprehensive Dose Model and Computer Code for Inhaled Radioactive Particles, Part I of Final Report of Radiological Safety Studies for the SNAP Program for Safety Branch, SEPO, USAEC, Environmental Safeguards Division, NUS Corporation, Rockville, Maryland (1969), Report No. NUS-596.

(3) J. R. Coleman and L. J. Perez, Jr., Considerations of a Tumor Probability Function and Micro-Dosimetry for the Deep Lung, Part II of Final Report of Radiological Safety Studies for the SNAP Program for Safety Branch, SEPO, USAEC, Environmental Safeguards Division, NUS Corporation, Rockville, Maryland (1969), Report No. NUS-596.

(4) J. P. McBride, Laboratory Studies of Sol-Gel Processes at the Oak Ridge National Laboratory, Oak Ridge National Laboratory Report No. ORNL-TM-1980 (1967).

(5) M. J. Fulwyler, US Patent Application Serial No. 123362(70), March 1971.

(6) M. J. Fulwyler and L. S. Cram, Model Particles for Automated Systems of Cell Analysis, J. Histochem. Cytochem. 18:677 (1970), Abstract No. 15.

(7) W. L. Hendry, A Volterra Integral Equation of the First Kind (in preparation).

(8) L. C. Northcliffe, Passage of Heavy Ions through Matter, Ann. Rev. Nucl. Sci. 13:67-102 (1963).

(9) Committee on Nuclear Science, Studies in Penetration of Charged Particles in Matter, National Academy of Sciences-National Research Council Publication No. 1133 (1964).

(10) L. M. Holland, G. A. Drake, J. E. London, and J. S. Wilson, Intravenous Injection with a Pulsed Dental Cleaning Device, Laboratory Animal Science 21:913-915 (1971).

(11) P. F. Mullaney and J. R. Coulter, An Electronic Particle Counting and Dispensing Device for Use in Animal Injection Experiments, Rev. Sci. Instr. 42:1434-1436 (1971).

(12) C. L. Sanders, R. C. Thompson, and W. J. Bair, Carcinogenesis of the Lung from Inhalation of Radioactive Particles, Battelle Memorial Institute, Pacific Northwest Laboratory, Richland, Washington (1969); available from U. S. Naval Radiological Defense Laboratory, San Francisco, California, Report No. NRDL-TRC-69-8.

(13) E. E. Underwood, Quantitative Stereology, Addison-Wesley Publishing Co., Reading, Massachusetts (1970), p. 84.

BIOPHYSICS SECTION

INTRODUCTION

The work of the Biophysics Section falls into four interrelated categories: (1) cell analysis and sorting instrumentation development; (2) biological applications of cell analysis and sorting; (3) physical radiobiology; and (4) computer applications and engineering support. This annual report will describe some of the work in the first three categories. The support in electronics and mechanical engineering, which comprises the fourth category, is crucial to many projects throughout the Biomedical Research Group. It involves four people (Carr, Butler, Perrings, and Larkins) but will not be discussed further for the purposes of this report.

The Biophysics Section of Group H-4 has pioneered in the development and invention of high-speed, flow-system methods of cell analysis and sorting. The motivation has been the belief that modern experimental physics could supply new and useful ways of obtaining important biological information on cell populations and their response to radiation. These efforts have resulted in (1) improved Coulter volume spectrometry; (2) invention of electronic cell sorting; (3) development of flow microfluorometry; (4) deeper understanding of light scattering by cells; (5) development of two-parameter cell analysis; and (6) invention of multiparameter cell sorting. In 1971, work has concentrated on the last four categories. Flow microfluorometry has been in routine biological use during the year and, in addition, factors limiting instrumental resolution and contributing to artifacts in cellular DNA distributions have been determined. The instrumentation introduces a total coefficient of variation of less than 2 percent for bright dyes like acriflavine-Feulgen, where photon statistical effects are minimal. Light-scattering theory has been investigated thoroughly by computer calculations based on Mie theory and a model which considers the cell as a sphere with a concentric nucleus. Experimental verification is in progress, and results to date support the theory. Applications to flow-system analysis have been initiated in the form of a two-parameter cell analyzer based on fluorescence and light scatter. Development of multiparameter cell sorting has progressed to the point where the system includes a bicolor (red and green) fluorescence sensor unit and a Coulter sensor. A scatter sensor can be added later. Tests of technical performance and experiments with a variety of cell populations have begun and will continue for several months. A second, simplified sorter dedicated exclusively to biological use and taking advantage of accumulated experience will be designed and built in the last half of this year.

Biological applications of cell analysis and sorting have included cooperative experiments with many scientists in Group H-4, mutual interest projects with the National Institutes of Health and U. S. Department of Agriculture, and cooperative experiments with a substantial number of scientists from other laboratories who have expressed interest in our unique facilities. Cooperative experiments with Group H-4 scientists have included DNA constancy in heteroploid cell lines, investigation of cell-surface binding sites with fluorescein-conjugated concanavalin A, life-cycle analysis by flow microfluorometry compared with the labeled DNA precursor method, cell survival and life-cycle analysis following gamma irradiation, effect of chemotherapeutic agents on DNA condensation and life cycle, exploration of histochemical techniques for histones, total protein and RNA, and investigation of the perturbation index (or drag fraction) in CHO cell populations. Mutual interest projects with other agencies involve ploidy monitoring in cell-culture systems, cancer screening, and animal disease diagnosis by immunofluorescence. An increasing list of scientists from other institutions have initiated interactions with us on

problems of common interest; these include the University of Colorado; Colorado State University; Max-Planck Institute for Biophysical Chemistry in Gottingen, Germany; Salk Institute for Biological Studies; University of New Mexico; Stanford University; University of Florida; and University of Wisconsin.

In the area of physical radiobiology, efforts include plutonium lung counting, tumorigenicity of highly radioactive particles, meson radiobiology, and computer applications to a wide variety of problems in Group H-4. The first of these projects will be described in this report. A lung counter has been developed at Los Alamos which has the capability of detecting about one-third of a maximum permissible lung burden (16 nCi) of plutonium-239. This counter has been used also to measure lead-210 in the skull of uranium miners.

CELL ANALYSIS AND SORTING INSTRUMENTATION DEVELOPMENT (A. Brunsting, J. R. Coulter, L. S. Cram, D. M. Holm, J. L. Horney, P. F. Mullaney, A. Romero, J. A. Steinkamp, T. T. Trujillo, M. A. Van Dilla, and W. T. West)

An Improved Instrument for Quantitative Cellular Fluorescence Measurements on Single Cells

The advent of flow systems for making high-speed measurements on single cells (1-7) has resulted in considerable interest in such quantities as DNA content per cell as a function of chromosome number (8,9), volume of the cell, or presence of fluorescent antibodies. As a result of biological experiments already performed with the use of this type of equipment, many experimenters are now considering using this valuable technique for performing a wide variety of biological experiments.

It is possible to quantitate a large number of physical-cellular parameters for which there is a known relationship between the dye and quantity being measured. We have found the system to be useful for basic research and potentially useful for disease diagnosis. For example, it has considerable potential in the whole area of the fluorescent antibody technique. The instrument considered here is an improvement of that deacribed by Van Dilla et al. (1) and has been used for nearly two years in routine biological experiments. Single-cell suspensions are stained with a dye which is specific for a given cellular moiety. Cells are caused to pass through a laser beam which excites the fluorescent dye and causes a flash of fluorescent light proportional to the amount of dye present in the cell. This flash of light is converted into an electric voltage pulse whoae amplitude is proportional to the amount of light from the cell and, hence, to the amount of material-binding dye. A histogram showing the number of cells with a given fluorescence is accumulated on a pulse-height analyzer, and the analysis of this pulse-height distribution enables the experimenter to determine the quantitative distribution of the dye within the cells. From this distribution and the relationship between the dye and quantity being measured, the experimenter can deduce the quantitiea of interest.

A schematic diagram of flow microfluorometer Model II (FMF II) is shown in Fig. 1. The cell suspension is pulled through a 0.5-mm inside diameter hypodermic tube at the bottom of the flow cell. A distilled water sheath flow surrounds this hypodermic tubing. The combined flows at this point are 3.2 mm in diameter. While maintaining laminar flow conditions, the combined flows are reduced in diameter to 250 μm, where it exits into a quiescent water volume and there intersects the laser beam. The combined flow exits through a nozzle and is collected into a water trap on a 360-mm mercury vacuum system. A Coherent Radiation argon-ion laser Model 54, normally set on the 476-nm line for Auramine-O dye, is used as the source of blue exciting light. The laser beam is focused to an elliptical cross section at the cell stream; beam power is monitored with a Jodon Model 450A. The fluorescent signal is collected with a projector lens having f/1.6 optics and, following the first projector lens where the light is parallel, a Corning glass filter (catalog No. 3-70) is used to block scattered light. A similar second projection lens focuses the fluorescent light to a pin hole whose diameter is 200 μm. After passing through the pin hole, the light is again made parallel by a small collimating lens. A prism is used to reflect the

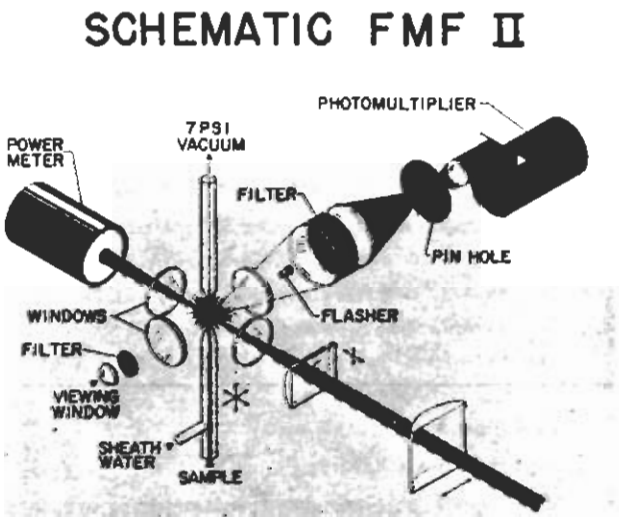

Fig. 1. Schematic diagram of the flow microfluorometer. The argon-ion laser beam comes from the lower right-hand corner and is focused by 20- and 2-cm focal length cylindrical lenses to an elliptical cross section 7 x 100 μm (width or height of the laser beam at half maximum intensity) at the intersection with the sample stream.

light into the photocathode of the RCA 4526 photomultiplier. This optical system utilizes darkfield illumination and has a magnification of 1. Thus, only light generated in the region of the intersection of the laser beam and cell stream is efficiently collected by the photomultiplier. A viewing window with a blocking filter to cut out the blue laser light is located opposite the photomultiplier and is used for alignment of the system. For normal alignment the only adjustments necessary are a horizontal sweeping of the laser beam across a fluorescent dye stream by moving the 20-cm focal length cylindrical lens and monitoring the direct current light level in the photomultiplier. This is optimized so that the experimenter can be assured that the cell stream is intersecting the maximum of the laser beam. Because the laser beam normally has an approximately Gaussian intensity distribution, it is necessary to make certain that intersection of the laser beam and cell stream is at the peak of the Gaussian distribution.

Attempts have been made to understand thoroughly and to minimize any errors or artifacts introduced by the instrumentation. Considerable progress has been made in understanding sources of error or perturbations in the signals caused by the instrument. Figure 2 shows a pulse-height distribution from exponentially-growing Chinese hamster ovary (CHO) cells. These cells were stained with Auramine-O using the Feulgen procedure to stain the DNA (10). The abscissa is proportional to the amount of fluorescence in the cells, and the ordinate is the number of cells having that amount of fluorescence. The largest peak to the left corresponds to cells in the G_1 state of their life cycle; the coefficient of variation of this peak is 5 percent. At present it is not known what percentage of this variation is due to actual variability in DNA content in the cells and what part is caused by the instrumentation, but it is expected, based upon the analysis of results so far obtained, that approximately half of the coefficient of variation in this figure is caused by instrumentation effects. To better understand these effects, a series of experiments have been done to localize the causes. The coefficient of variation of this G_1 peak can be a good measure of the quality of the instrument if there is reason to believe that the cells do not have significant variations in their DNA content. This is the case of CHO cells and, for this reason, they have been used along with plastic microspheres (11) containing dye to monitor instrumentation effects. Each component of the entire system has been tested and optimized for the instrumentation configuration shown in Fig. 1.

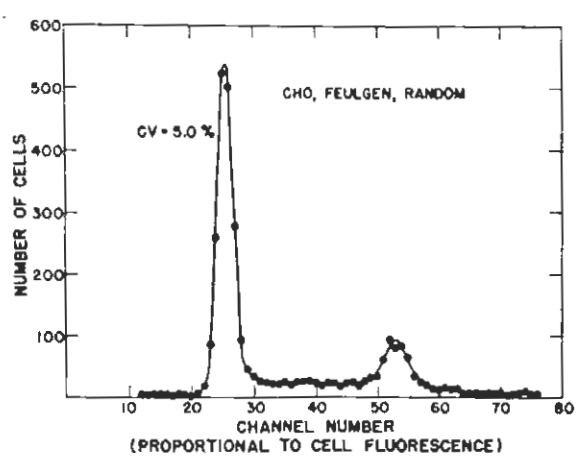

Fig. 2. Feulgen-DNA distribution of Chinese hamster ovary cells growing asynchronously in suspension culture.

One of the first considerations was to measure the amount of light coming from the cells as a function of laser power. The purpose of this experiment was to look for any evidence of the dye being saturated by the intense blue laser light. Curve A of Fig. 3 shows a plot of the amount of light coming from the cells as a function of laser power (see following page). These experiments were done with a Model 52G Coherent Radiation laser, which has 10 times the power of the Model 54. It is obvious that no dye saturation effects are evident as the data fall on a 45° slope on log-log paper. Because saturation effects were not observed, the next step was to measure the coefficient of variation of the cells as a function of laser power. To assist in these measurements, a light flasher was introduced in the optical path so that pulses of an amplitude equal to that of the cells could be generated. In these experiments cells were run through the flow system, and the pulse-height distribution was obtained. The flasher was then adjusted to produce a peak in the same channel as that for the cells, and the coefficient of variation of this peak was determined. The plot of these two sets of data is

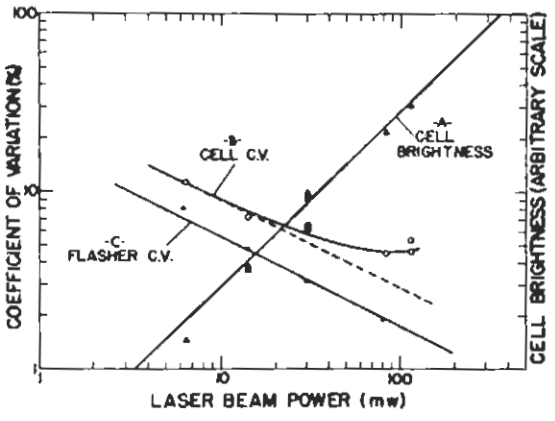

Fig. 3. Brightness of cells as a function of laser beam power (A), indicating no dye saturation effects. Coefficient of variation of the G_1 peak of CHO cells as a function of laser beam power (B), indicating that statistical effects for Auramine-O stained cells are significant at lower power and that laser beam instability is significant at higher power. Coefficient of variation of a photodiode flasher of brightness equal to stained cells as a function of laser beam power (C), indicating light expected from statistical effects. It indicates that photon statistical effects are important with this stain.

also shown in Fig. 3 (curves B and C). The most significant feature of this plot is that of the flasher slope. The straight line drawn through those points has the proper slope for purely statistical effects, which are caused by variation in number of photoelectrons emitted at the photocathode of the photomultiplier tube. Thus, for Auramine-O stained cells the light signal reaching the photomultiplier is weak enough so that this statistical fluctuation is a significant factor in the coefficient of variation. Cells also follow this same slope at low power; however, at higher power they deviate significantly from this slope. The absolute difference between the flasher curve and cell curve is caused by a number of things. One of them is the intrinsic variation in DNA per cell. Another is the variation introduced by the staining procedure. Another is the variation in laser beam intensity as a function of position and as a function of time. The electronic effects are insignificant at this time. The increase in coefficient of variation at the highest power is very likely caused by increased noise in the laser beam. Monitoring of the laser beam during these experiments was not done; however, subsequent experiments showed that the laser beam intensity fluctuates with time, and corrective measures are being taken to minimize this effect. The coefficient of variation for the flasher curve shows that statistical effects are significant with Auramine-O dye. Recent use of acriflavine, which is a much brighter dye, considerably improves the statistical effects.

The laser beam was shaped into an ellipse so that cells could be uniformly illuminated and that total fluorescent light signal would be short. For this instrument, the major axis of the ellipse has a full width at half the maximum light intensity of about 100 μm, while the minor axis of the ellipse has a full width at half maximum intensity of about 7.5 μm. These dimensions are obtained for the major and minor axes, respectively, by placing a 20-cm focal length cylindrical lens 28 cm from the cell stream and a 2-cm focal length cylindrical lens at its focal point. With this arrangement a complete scan of a cell takes place in 2 to 3 microseconds so that standard nuclear electronics equipment can be used.

It is possible to discriminate between two cells stuck together from one cell having twice as much DNA. This is quite important in making accurate analyses of the DNA distribution in cells where the number of tetraploid cells is desired with high accuracy. By making the laser beam small or on the order of a cell dimension, pulse-shape discrimination can be used to distinguish single cells from double cells. A fortunate feature of the laminar flow system is that alignment of two cells takes place in the flow system; therefore, two peaks separated by a saddle are observed when two attached cells pass the laser beam. For cells that come in time greater than 4 microseconds, a complete discrimination is made. However, when the laser beam is on the order of a cell dimension, it is necessary to use a pulse integrator to integrate the complete light from the passage of the cell. This integrated output is then analyzed by the pulse-height analyzer. Without this integrator an erroneous answer would be obtained.

Some investigations were made as to the effect

of cell stream diameter and nonuniformity of laser beam illumination. For these experiments cella were examined under normal conditions (i.e., 21 ml/min flow rate for the sheath water that surrounds the sample and 0.15 ml/min sample flow volume). This corresponda to a cell stream diameter of 15 μm at the laser beam intersection. Since this dimension is very nearly equal to actual cell diameter, there was very little uncertainty as to cell position in the laser beam. While the sheath flow was maintained at its normal laminar flow, the sample flow was increased up to 10 times normal, and the coefficient of variation was measured of cells in the G_1 peak. The concentration of cells was maintained low enough to eliminate accidental coincidences in the high flow rates. Cells with small coefficient of variation were used so that any changes from nonuniform illumination were obvious. Results of these experiments showed that 4 percent coefficient of variation was obtained for normal sample flow conditions and only 4.6 percent coefficient of variation for 10 times that flow. The higher flow corresponds to a 45-μm cell stream diameter. This shows rather convincingly that, under normal conditions, the laser beam illumination of the cell stream is very uniform.

Counting rates of the order of 1000 cells/sec are quite reasonable with this unit, and higher counting rates can be obtained since total trsnsit time of a cell is 3 microseconds and base-line recovery is within 20 microseconds. The quality of the instrument is demonstrated further by measuring the fluorescence distribution of very uniform 12-μm fluorescent plastic microspheres. Figure 4 illustrates the capabilities of the instrument to resolve two fluorescence distributions resulting from mixing two populations of microspheres differing in intensity by 10 percent. The two Gaussian distributions add mathematically, as expected. This demonstrates the importance of minimizing the instrumental contribution to the width of the distribution. Similar experiments indicate that two subpopulations can be reduced if modal fluorescence differs by at least 5 percent and if the fraction of one population is at least 10 percent of the total.

This instrument has been in routine use for biological experiments for about two years and has shown itself to be quite reliable. It can be

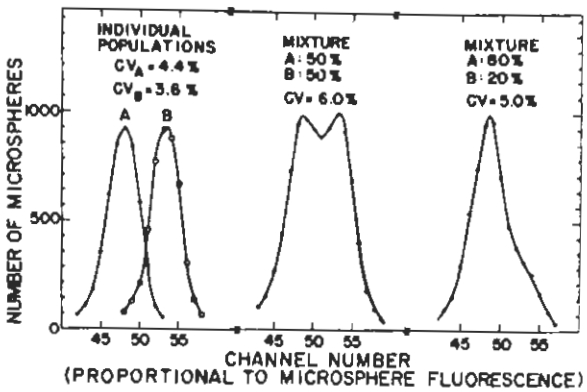

Fig. 4. Fluorescence distributions of uniform fluorescent plastic microsphere populations as individual populations (A) and (B), as 50:50 mixtures of (A) and (B), and as 80:20 mixtures of (A) and (B).

operated by a technician and has a wide variety of applications. It appears at this time that the major room for improvement is in obtaining a laser beam that is of uniform intensity as a function of time. Corrective action is being undertaken to eliminate this source of error. It appears that instrumental effects will be reduced to the neighborhood of 2 percent or less if brighter dyes are used and the laser can be improved further.

REFERENCES

(1) *M. A. Van Dilla, T. T. Trujillo, P. F. Mullaney, and J. R. Coulter, Science 163:1213 (1969).*

(2) *H. R. Hulett, W. A. Bonner, J. Barrett, and L. A. Herzenberg, Science 166:747 (1969).*

(3) *L. A. Kamentsky, In: Cytology Automation (D. M. D. Evans, ed.), E. and S. Livingstone, Edinbrough and London (1970), pp. 177–185.*

(4) *J. Schumann, F. Ehring, W. Gohde, and W. Dittrich, Arch. Klin. Exp. Derm. 239:377 (1971).*

(5) *E. Sprenger, N. Bohn, and W. Sandritter, Histochemie 26:238 (1971).*

(6) *L. L. Wheeless and S. F. Patten, Jr., Acta Cytol. 15:111 (1971).*

(7) *F. E. Holly and A. Norman, Exp. Cell Res. (1972), in press.*

(8) P. M. Kraemer, D. F. Petersen, and M. A. Van Dilla, Science 174:714 (1971).

(9) P. M. Kraemer, L. L. Deaven, H. A. Crissman, and M. A. Van Dilla, In: Advances in Cell Biology, Vol. 2 (E. J. DuPraw, ed.), Academic Press, Inc., New York (1972), in press.

(10) T. T. Trujillo and M. A. Van Dilla, Acta Cytol. 16:26-30 (1972).

(11) L. S. Cram, M. J. Fulwyler, and J. D. Perrings, In: Abstracts of the 15th Annual Meeting, Biophysical Society, New Orleans, Louisiana (February 15-18, 1971).

Differential Light Scattering: A Possible Method of Mammalian Cell Identification

We have been interested in the light-scattering properties of nearly spherically-symmetric mammalian cells as a possible means of identification, as suggested by Wyatt in the case of bacteria (1). Calculations based on the theory of Lorenz (2), commonly called Mie theory (3), for a homogeneous sphere indicate that small-angle scattering can yield information on whole-cell size (4). For these calculations, a mammalian cell was imagined to be a homogeneous sphere immersed in a water-like medium so that the relative refractive index of the cell was slightly greater than unity. A more realistic model for some mammalian cells is a homogeneous sphere (nucleus) of one refractive index surrounded by a concentric, homogeneous coating (cytoplasm) of a slightly lower refractive index. An example of this type of cell is the Chinese hamster ovary cell (5), line CHO. CHO cells are about 12 μm in diameter with nuclei whose diameters are about 8 μm.

The cytoplasm of normal mammalian suspension cells is surrounded by a distinct, definite membrane as is its nucleus. For this reason, a coated sphere with its sharp, distinct optical boundaries was selected as a model. So that the possible effects of internal structure on scattering patterns of suspension cells could be predicted and understood, calculations were performed for this coated sphere model. In Fig. 1 some representative stained (6) CHO cells in various parts of their life cycle, stained with pinacyanol to bring out chromosome detail, are presented. The photograph of stained

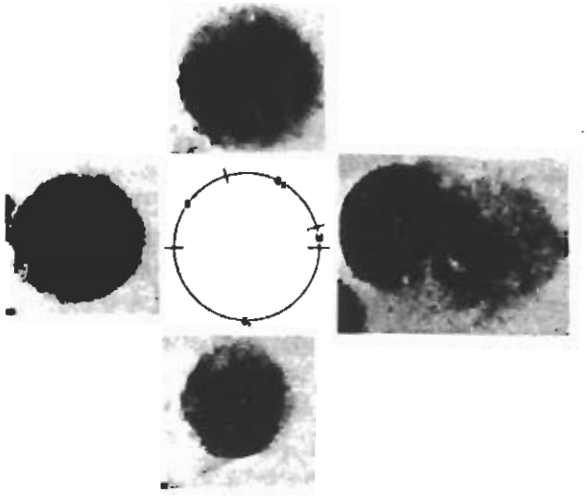

Fig. 1. Stained Chinese hamster ovary cells at various portions of their life cycle (see text for definitions of G_1, S, G_2, and M). Note that cells in M (mitosis) are not only larger than the young daughter cells in G_1 but have considerably more complex nuclear structure.

cells does not reflect accurately either the nuclear and plasma membranes or the exact optical properties of unstained cells; rather, the stain shows the gross volume morphology of the cell and its nucleus around its life cycle.

In the G_1 part of its life cycle, just after division, the cell is about 12 μm in diameter (on the bottom, Fig. 1). As the cell moves through S, when DNA synthesis occurs (on the left side, see Fig. 1), and into G_2 and M, just before division (on the top and right side, Fig. 1), its volume increases to about twice the volume of the G_1 cell or a diameter of about 15 μm. The generation time, or one complete traversal of the circle in Fig. 1, takes about 17 ± 2 hours. The lengths of these labeled sections of arc are proportional to their respective life-cycle parts. The availability of CHO cells, their spherical structure, and similarity to other interesting mammalian cells make this cell line a worthwhile model system. A cell line such as the CHO will certainly have much greater complexity than the coated sphere assumed here, but the anticipation is that certain trends in scatter patterns of real cells can be predicted and understood with this model.

Calculations used here, based on the model of Aden and Kerker (7), are described in detail elsewhere (8) and will not be repeated here. Following

the notation of Kerker (9), the parameters of interest are described below. Let the inner sphere have a radius $\underline{a}$, a size parameter $\alpha = 2\pi\underline{a}/\lambda$ where λ is the wavelength of the light in the surrounding medium, and a refractive index $\underline{m}_1$, relative to the homogeneous isotropic and non-absorbing medium. Let the concentric coating have an outside radius $\underline{b}$, a size parameter $\nu = \frac{2\pi\underline{b}}{\lambda}$, and a relative refractive index $\underline{m}_2$; in general, $\underline{m}_1$ and $\underline{m}_2$ can be complex to account for absorption. Both the sphere and coating are homogeneous and isotropic. The intensity function of the scattered light, $\underline{i}_1$, has its electric field vector polarized perpendicular to the scattering plane. The experimental measured intensity with this polarization is proportional to $\underline{i}_1$. The scattering angle θ, defined so that $\theta = 0°$, corresponds to forward scattering and $\theta = 180°$ to back-scattering. The $\underline{m}'$ is volume average of the refractive indices $\underline{m}_1$ and $\underline{m}_2$.

Kattawar and Plass (10) have investigated the width of the forward scatter lobe as a function of size parameter, x, and refractive index ($x = \pi d/\lambda$, where d = particle diameter, λ = incident wavelength), for nonabsorbing homogeneous spheres. They plotted the angle, θ, at which $\underline{i}_2(\theta) = \underline{i}_2(0°)/2$ as a function of x, where $\underline{i}_2$ is proportional to the measured scattered intensity with its E vector polarized parallel to the scattering plane. They found that, for refractive indices as low as 1.01, the half-width of $\underline{i}_2$ was proportional to $1/x$ for $x \gtrsim 3$, which agrees with the Fraunhofer diffraction model.

We have done an equivalent computation for the coated sphere, and the results are shown in Fig. 2. The vertical axis is log θ, and the horizontal axis is log ν, the whole-cell size parameter. The diffraction model result is indicated by the straight line; the various symbols refer to different refractive indices equal to the range of live and fixed CHO refractive indices: $\underline{m}_1/\underline{m}_2 = 1.04/1.02$ to $1.10/1.07$, where subscripts 1 and 2 refer to the nucleus and cytoplasm, respectively. The nuclear size parameter, α, is $2\nu/3$. For $\nu \lesssim 3$ the points deviate from the diffraction line and approach $\theta = 45°$, as Kattawar and Plass observed. In this region the diameter of the whole-cell is less than wavelength, and diffraction should not apply, whereas for $\nu > 3$ the points cluster about the diffraction

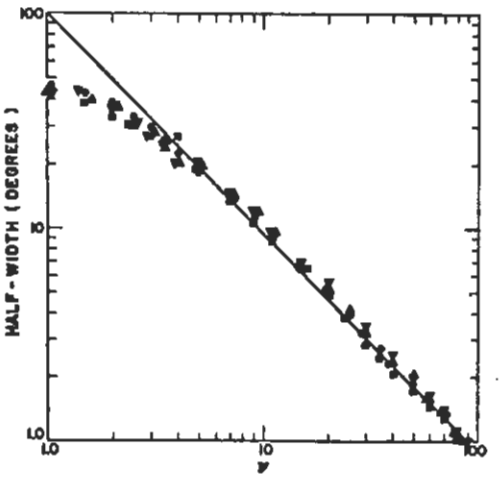

Fig. 2. Log-log plot of the half-width of the intensity function $\underline{i}_2$ versus ν, the whole particle size parameter. For this case, the core size parameter $\alpha = 2\nu/3$. The various core ($\underline{m}_1$) and coating ($\underline{m}_2$) refractive indices are: $\underline{m}_1/\underline{m}_2 = 1.04/1.02$ (■); $\underline{m}_1/\underline{m}_2 = 1.05/1.03$ (▼); $\underline{m}_1/\underline{m}_2 = 1.07/1.05$ (○); and $\underline{m}_1/\underline{m}_2 = 1.10/1.07$ (▲). The straight line is the diffraction result.

line. Similar results were obtained for $\alpha/\nu = 0.2$, ... 0.8. These results indicate that diffraction is the main scattering mechanism in the forward lobe, even in the case of a coated sphere. Thus, forward scattering measurements should reflect gross size and be insensitive to internal atructure.

Small-angle light-scattering meaaurements have been made on CHO cells after mitotic synchronization (11,12) with the photometer deacribed elsewhere (13). It has been shown that, although there are profound internal structure differences between G_1 and M cells (cf. Fig. 1), the small-angle light-scattering signal is responsive to gross size as expected on the basis of Fig. 2.

In Fig. 3 we see a semi-log plot of $\underline{i}_1$ versus θ for both the homogeneous sphere (HS) and coated sphere (CS), see following page. The coated sphere (bottom curve, Fig. 2) has typical CHO parameters ($\alpha = 2\nu/3$, $\nu = 86$, $\lambda = 0.47$ µm, $\underline{m}_1 = 1.05$, $\underline{m}_2 = 1.03$), and the homogeneous sphere (top curve, Fig. 4) has a size parameter of 86 and a refrsctive index equal to the volume average of the refractive indices of the coated sphere, equal to 1.036. The shape and magnitude of the two curves within the forward lobe ($\theta \lesssim 1.5°$) are essentially the same, which is in agreement with the above discussion concerning

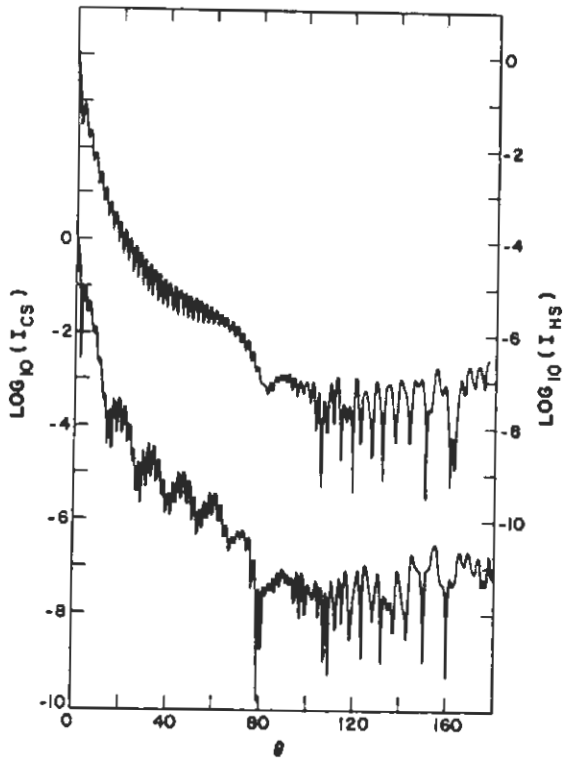

Fig. 3. Semi-log plot of the intensity function $\underline{i}$ versus θ for a coated sphere with α = 2ν/3, ν = 86, $\underline{m}_1$ = 1.05, $\underline{m}_2$ = 1.03 (bottom curve), and a homogeneous sphere with α = ν = 86, $\underline{m}'$ = 1.036. The coated sphere (I_{CS}) scale is on the left and the homogeneous sphere (I_{HS}) scale on the right. The scales have been displaced for clarity.

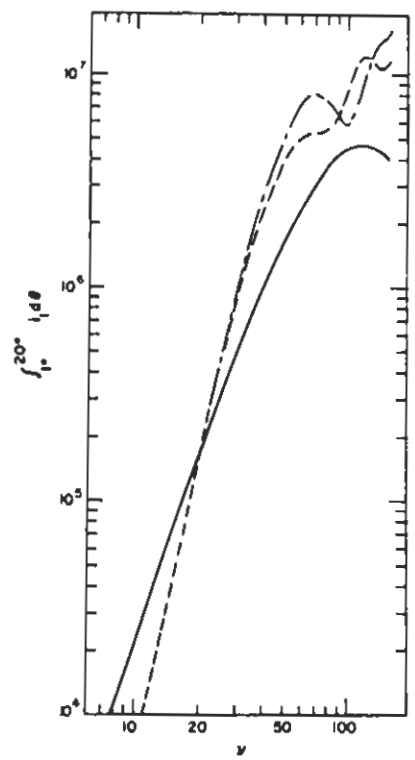

Fig. 4. Log-log plot of $\int_{1°}^{20°} \underline{i}_1\ (\theta)\ d\theta$ versus ν for a coated sphere (-----), a homogeneous sphere (— — —), and a diffraction (———) versus ν (i.e., the total volume size parameter). For the coated sphere α = 2ν/3, $\underline{m}_1$ = 1.05, $\underline{m}_2$ = 1.03. For the homogeneous sphere, $\underline{m}'$ = 1.036.

diffraction. However, these features should alao be noted: (a) the first minimum of both curves is an order of magnitude deeper for CS and HS; (b) a periodicity of the fine structure of about 12° exists for CS, whereas the HS has no such periodicity for $1.5° \lesssim \theta \lesssim 80°$; (c) the structure of the two curvea is quite different for $80 \lesssim \theta \lesssim 180°$, although the average value of both curves is about the same; and (d) the pronounced minima outside the general area of the forward lobe in the CS caae suggest this angular region as an interesting one to study in more detail.

Details of this angular region are examined in Figs. 4 and 5. In Fig. 4 the intensity function $\underline{i}_1$ integrated from θ = 1° to θ = 20° for the case of HS, CS, and the perfectly absorbing sphere (diffraction theory) versus the whole-cell size parameter (ν in the case of GS) is plotted. The CS has parameters which are typical of an interphase CHO

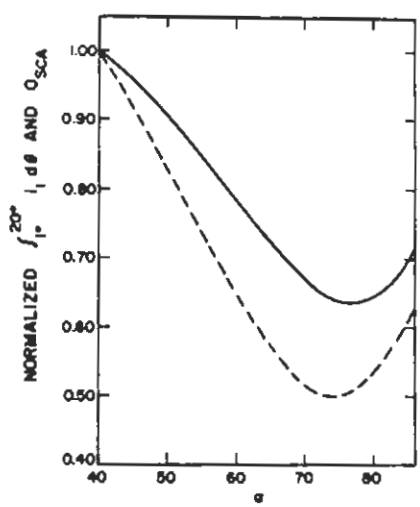

Fig. 5. Comparison of Q_{sca} (———) and $\int_{1°}^{20°} \underline{i}_1\ (\theta)\ d\theta$ (-----) versus α for ν = 86, $\underline{m}_1$ = 1.05, and $\underline{m}_2$ = 1.03. Both curves have been normalized at α = 40.

cell: $\nu = 86$, $\alpha = 2\nu/3$, $\underline{m}_1 = 1.05$, $\underline{m}_2 = 1.03$; the HS has $\alpha = \nu = 86$ and $\underline{m}' = 1.036$. Thus, diffraction theory, which takes no account of either the internal details or the refractive index of the scatterer, does not compare well with the HS or CS models in this situation. This is not the case in the forward lobe, as we saw in the discussion above (i.e., the three models produce very similar results, cf. Fig. 2). Note that there is a substantial difference between the coated and homogeneous spheres in the outside size parameter region of about 40 to 90. CHO cells illuminated by 0.47 μm light fall in this whole-cell size parameter region. This implies that coated spheres with parameters similar to CHO cells can be differentiated from homogeneous spheres with a volume average refractive index and size parameters similar to CHO cells in their $\underline{i}_1$ patterns between 1° and 20°. Hence, in this case, these two models with the same gross volume but different internal details produce significantly different intensity patterns.

Suppose the whole-cell size is constant with only a variation of nuclear size. This is the case considered in Fig. 5, where $\underline{m}_1$ and $\underline{m}_2$ are the same as in Fig. 3. In the case of CS, α varies from 40 to 86 and $\nu = 86$ -- parameters which are again close to the CHO situation. This graph shows the integrated intensity from 1° to 20° and Q_{sca} (equal to the extinction efficiency factor in this case of no absorption) versus nuclear size, both normalized at $\alpha = 40$. Q_{ext} is proportional to the total amount of energy removed from the incident light beam due to scattering and absorption (since absorption in this case is zero, only scattering need be considered). The normalizing factor is 1/2.55 for the Q_{sca} curve and $1/8.61 \times 10^6$ for the integration curve. Q_{sca} is proportional to the total energy extracted from the main beam from all causes, since there is zero absorption. Q_{sca} follows the integrated intensity quite closely in the parameter range of interest, indicating the 1° to 20° range contains a large percentage of total scattered light which, in turn, reflects core size.

Van de Hulst (14) has studied extensively and explained the behavior of Q_{ext} as a function of size parameter and refractive index. Basically, a minimum exists at $\alpha \simeq 75$ in Fig. 5 because of Huygen's construction of the incident plane wave in the shadow of the scatterer produces destructive interference with the radiation passing through the scatterer.

From the discussion on scattering in the forward lobe, the coated aphere model predicts that in this region diffraction is the major scattering mechanism for $\nu < 3$ (the region where the whole particle diameter is less than incident wavelength), even for coated spheres of low relative refractive indices. Hence, scattering intensity measurements made in the forward lobe should be insensitive to cellular internal structure and should reflect gross size. Data on CHO cells support this result (13).

The interesting prediction of these calculations is that light-scattering measurements from concentrically-spherical types of cells which are made outside the forward lobe may reflect internal structure and permit an estimation of nuclear size to be made. Two properties of cells may then be approachable by light-scattering techniques which may permit identification of cell types, assuming that $\underline{m}_1$ and $\underline{m}_2$ are not broadly distributed for a given cell population: gross size (forward lobe) and nuclear size (beyond the forward lobe).

In order to test these theoretical predictions, several experiments on suspensions of mammalian cells are planned. A film photometer has been designed and constructed and is currently undergoing tests. In this device, a standard light-scattering cuvette containing a sample suspension is placed at the center of a light-tight drum 2.5 feet in diameter. Film is wrapped around the inside circumference of the drum. The cuvette is illuminated by light from a 5-mW helium-neon laser, and the light scattered between 3° and 177° is recorded on the film, which is read with a microdensitometer after development. Preliminary runs have been made with 10-μm polystyrene spheres with a volume coefficient of variation of 3 percent. Results on these spheres are being compared with experiments made with a commercial light-scattering difference (Differential I, Science Spectrum, Santa Barbara, California). The film photometer offers greater sensitivity and resolution in that more scattering structure is observable with the film photometer. Experiments with cells will commence when our present film calibrations are complete.

REFERENCES

(1) P. J. Wyatt, Differential Light Scattering: A Physical Method for Identifying Living Bacterial Cells, Applied Optics 7:1879-1896 (1968).

(2) L. Lorenz, Oeuvres Scientifiques 1:405-497; Librairie Lehmann and Stage, Copenhagen (1898).

(3) G. Mie, Beitrage zur Optik truber Medien, Speziell Kolloidaler Metallosungen, Annal. Physik 25:377-409 (1908).

(4) P. F. Mullaney and P. N. Dean, The Small Angle Light Scattering of Biological Cells, Biophys. J. 10:764-772 (1970).

(5) J. H. Tjio and T. T. Puck, Genetics of Somatic Mammalian Cells. II. Chromosomal Constitution of Cells in Tissue Culture, J. Exp. Med. 108:259-271 (1958).

(6) H. P. Klinger and D. O. Hammond, Rapid Chromosome and Sex-Chromatin Staining with Pinacyanol, Stain Techn. 46:43-47 (1971).

(7) A. L. Aden and M. Kerker, Scattering of Electromagnetic Waves from Two Concentric Spheres, J. Appl. Phys. 22:1242-1246 (1951).

(8) A. Brunsting and P. F. Mullaney, Light Scattering from Coated Spheres: A Model for Biological Cells, Applied Optics (1972), in press.

(9) M. Kerker, The Scattering of Light and Other Electromagnetic Radiation, Academic Press, Inc., New York, N. Y. (1969).

(10) G. W. Kattawar and G. N. Plass, Electromagnetic Scattering from Absorbing Spheres, Applied Optics 6:1549-1554 (1967).

(11) R. A. Tobey, E. C. Anderson, and D. F. Petersen, Properties of Mitotic Cells Prepared by Mechanically Shaking Monolayer Cultures of Chinese Hamster Cells, J. Cell. Physiol. 70:63-68 (1967).

(12) D. F. Petersen, E. C. Anderson, and R. A. Tobey, In: Methods in Cell Physiology, Vol. III (D. M. Prescott, ed.), Academic Press, Inc., New York, N. Y. (1968).

(13) P. F. Mullaney, M. A. Van Dilla, J. R. Coulter, and P. N. Dean, Cell Sizing: A Light Scattering Photometer for Rapid Volume Determination Rev. Sci. Instr. 40:1029-1032 (1969).

(14) H. C. Van de Hulst, Light Scattering by Small Particles, Wiley and Sons, New York, N. Y. (1957), p. 173ff.

Multiparameter Cell Analysis and Sorting

During the past several years, the Biophysics Section has been developing new instrumentation techniques for application to high-speed analysis and sorting of biological cells in suspension. Past and current efforts in this area have resulted in (a) an improved cell volume spectrometer; (b) a flow microfluorometer for measurement of cellular DNA and other properties characterized by fluorescent stains; (c) a light-scatter photometer for optical cell sizing; and (d) an electronic technique for sorting cells based on cell volume. We are developing currently a multisensor cell analysis and sorting system for use in cell biology research and medical applications, such as cancer cell identification. This system is expected to be of increased usefulness as it will not only allow one to measure several physical and chemical properties of cells but also to physically isolate particular cells for subsequent examination. Multiparameter analysis greatly enhances the ability to discriminate or select a particular cell subpopulation from a heterogeneous mixture.

Cells stained using fluorescent compounds in aqueous suspension are introduced into a new dual-sheath flow chamber wherein electronic and optical sensors measure cell volume, fluorescence, and light scatter as illustrated in Fig. 1 (see following page). The cell suspension is introduced into the flow chamber through a platinum sample inlet tube, which also serves as the volume-sensing electrode. Flowing around the sample inlet tube and enveloping the cell stream is a particle-free sheath liquid (Sheath No. 1). Because flow is laminar, the streams do not mix but move as one through a Coulter volume-sensing orifice, wherein cell volume is electrically measured. Since cells are confined centrally as they pass through the volume-sensing orifice, volume resolution is improved (1). Cells next enter a viewing region via a second sheath fluid, where they intersect an argon-ion laser beam causing light scatter and fluorescence. Scattered light provides quantitative information on cell size and possibly morphology (2,3); fluorescence is a quantitative measure of cell constituents to which the fluorescent dye is bound [e.g., Feulgen-DNA (4)]. Light scatter and fluorescence are, in turn, measured

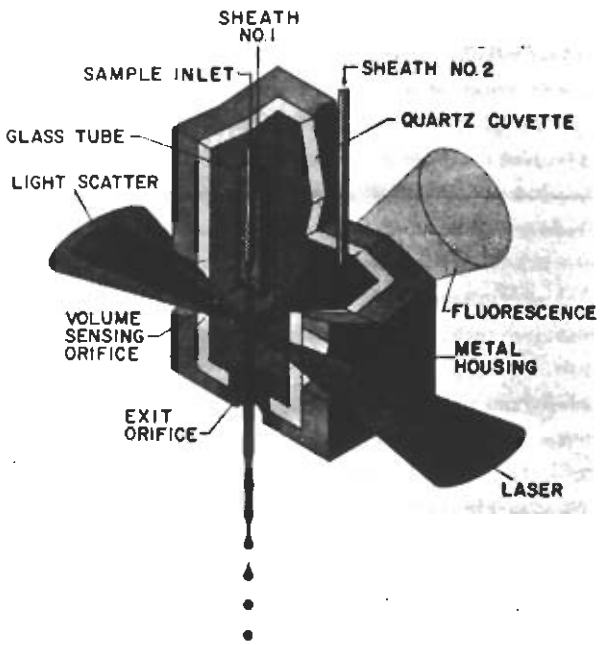

Fig. 1. Cut-away view of the flow chamber.

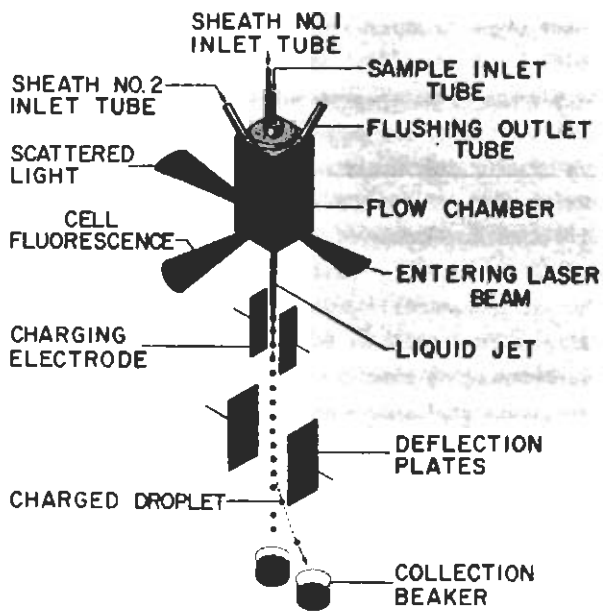

Fig. 2. The multisensor cell separator.

by electro-optical sensors, the fluorescence sensor being a dual-photomultiplier array which measures fluorescence in two distinct wavelength bands. The second sheath fluid serves to reduce the effect of pressure drop created by the Coulter volume-sensing orifice (75 μm diameter), facilitating droplet formation. After passing the laser beam, the cell suspension jets out into air from a coaxially-aligned exit nozzle. A piezoelectric crystal transducer mechanically coupled to the flow chamber, driven electrically at a frequency of 40 to 60 kHz, is used to produce uniform liquid droplets by regularly disturbing the emerging jet, as shown in Fig. 2. The droplet-charging and deflection schemes are similar to the original cell sorter invented at this Laboratory (5).

Signals from the volume, fluorescence, and light scatter sensors are fed directly to the multiparameter signal-processing unit for analysis and routing (Fig. 3). Presently the multiparameter signal-processing unit serves as the central electronic processing unit for cell analysis and sorting.

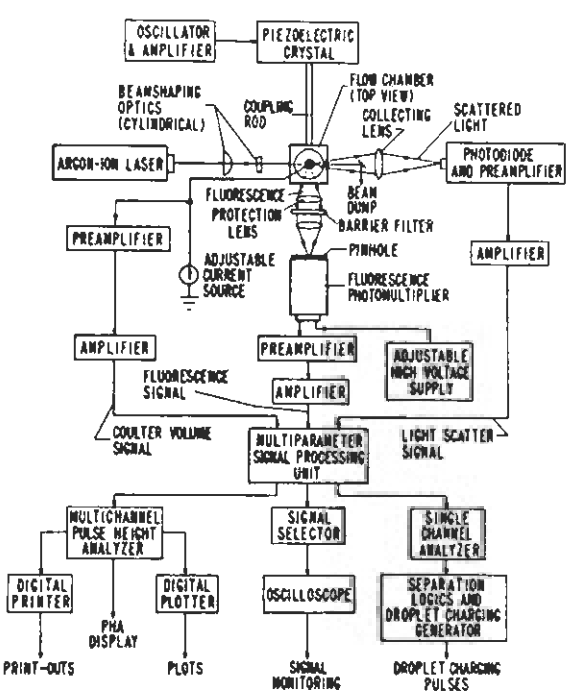

Fig. 3. A system block diagram.

Signals received by the processing unit can be processed in a variety of ways. For example, single-parameter analysis frequency distribution histograms of cell volume, fluorescence, and light scatter can be performed by individually processing these signals, which are routed to the multichannel pulse-height analyzer. Alternatively, signals from several sensors can be combined to form ratios (e.g., DNA-to-cell volume and frequency distribution histograms are recorded). Gated analysis of two or more parameters can also be performed. For example, the fluoreacence distribution histogram of all cells of a certain volume can be obtained. Outputs not shown in Fig. 3 are also provided by the multiparameter signal-processing unit for a two-parameter multichannel pulse-height analyzer for two-dimensional pulse-height analysis. The signal-processing unit also routes processed cell signals (e.g., single parameters, ratios, etc.) to the single-channel pulse-height analyzer to trigger cell sorting.

The first multiparameter flow chamber designed for high-speed cell analysis and sorting was completed in mid-1970. This unit was designed to demonstrate proof-of-principle [i.e., that sorting could be triggered by more than one sensor (optical, electrical)]. The experiment was successful; it was established that the multisensor analysis and sorting principle was valid. A complete prototype multisensor cell sorter was first operated in the latter part of 1971. A hard-wired multiparameter signal-processing unit was designed concurrently and first operated in mid-1971. As might be expected, this prototype experimental system has required considerable debugging, and at the same time many improvements of flow chamber, sample delivery method, electronics, and sorting mechanism have been made. A bicolor (green and red) fluorescence sensor-optical system has recently replaced the present single color fluorescence sensor. The dual fluorescence sensor has the added capability for either single or bicolor fluorescence using the metachromatic dye acridine orange. New cell separator control logics are being designed and constructed currently to permit more efficient cell separation. Design of a second multiparameter cell sorter system will begin toward the middle of 1972. This unit will be dedicated to biological experimentation, while the present sorter system will continue to be used for instrument development.

The status of multisensor sorter development in early 1972 is as follows. Experiments to test capability for simultaneous analysis of cell volume and fluorescence (Feulgen-DNA) have been accomplished on cultured Chinese hamster cells (CHO) and exfoliated squamous cells. Sorting of squamous cells on the basis of cell volume has been demonstrated. Coefficients of variation of 4 to 6 percent for the G_1 peak of CHO cells stained by the acriflavine-Feulgen procedure have been obtained.

Evaluation of system resolution, individual sensor performance, and multiparameter signal-processing techniques is presently underway using nonbiological test particles (fluorescent microspheres) and well understood cell populations. More interesting cell populations will soon be studied. These will include experiments with cell populations containing fluorescein-conjugated concanavalin-A bound to membrane surface sites, cells stained metachromatically with acridine orange (e.g., leukocytes), and cells from solid tumors and exfoliative cytology material. One aspect of the latter work will be determination of optimal detection parameters. Cell volume, DNA and RNA content, and nuclear-to-cytoplasmic ratios are to be investigated.

Experience to date in developing the present system has indicated areas for improvement and simplification of the next system, which will be dedicated to biological applications. Initial design work has started on the new sorter unit, with a completion date near the end of this year. At that time we will have two operating sorters: one for biology and one for instrumentation development.

REFERENCES

(1) J. T. Merrill, N. Veiades, H. R. Hulett, P. L. Wolf, and L. A. Herzenberg, An Improved Cell Volume Analyzer, Rev. Sci. Instr. 42:1157-1163 (1971).

(2) P. F. Mullaney and P. N. Dean, The Small Angle Scattering of Biological Cells, Biophys. J. 10:764-772 (1970).

(3) A. Brunsting and P. F. Mullaney, Light Scattering from Coated Spheres: A Model for Biological Cells, J. Appl. Optics (1972), in press.

(4) M. A. Van Dilla, T. T. Trujillo, P. F. Mullaney, and J. R. Coulter, Cell Microfluorometry: A Method for Rapid Fluorescence Measurement, Science 163:1213-1214 (1969).

(5) M. J. Fulwyler, R. B. Glascock, R. D. Hiebert, and N. M. Johnson, Device which Separates Minute Particles According to Electronically Sensed Volume, Rev. Sci. Instr. 40:42-48 (1969).

BIOLOGICAL APPLICATIONS OF CELL ANALYSIS AND SORTING

(L. S. Cram, H. A. Crissman, J. C. Hensley, D. M. Holm, D. F. Petersen, A. Romero, T. T. Trujillo, and M. A. Van Dilla)

Life-Cycle Analysis of Cells by Flow Microfluorometry and Labeled DNA Precursors

Many investigations dealing with periodic biochemical events or regulatory mechanisms controlling macromolecular biosynthesis are dependent upon precise temporal markers in the life cycle of mammalian cells. The cell cycle, first recognized by Howard and Pelc (1), consists of pre- and post-synthetic gaps (G_1 and G_2), the DNA-synthetic period (S), and the mitotic period (M). This terminology forms the basis for modern cell-cycle analysis and provides the temporal framework upon which biochemical events can be arranged.

A number of published techniques (2-4), based on unique biochemical or physical properties of cells in specific phases of the cell cycle, have been employed for life-cycle analysis. These methods are based either on the appearance of mitotic figures or on the occurrence of cell division; either parameter provides a measure of the progress of cells around the cell cycle. For example, if a random culture is pulsed with labeled thymidine, only S cells will be labeled so that, after an elapsed time equal to duration of G_2, the first labeled cells will reach mitosis (2). Statistical precision of measurement can be improved by accumulating the mitotic figures with a colcemid block. Scoring, which is tedious, must be performed visually under the microscope; as a compensation, the cells are evaluated individually in terms of their uptake of a specific precursor.

Development of flow microfluorometry (FMF) at the Los Alamos Scientific Laboratory has provided a new approach to life-cycle analysis. The operational features and instrumentation involved in this high-speed flow system have been described in detail elsewhere (5-8). Feulgen-DNA distributions of mammalian cells obtained by FMF analysis reveal distinctive distributions which depend upon cell distributions around the cell life cycle. A typical Feulgen-DNA distribution of exponentially-growing Chinese hamster ovary cells is shown in Fig. 1, together with the computer-fit data obtained from the cellular distribution. The data-processing program makes a least-squares best-fit of a normal distribution function to the G_1 peak, a second-degree polynomial to the S-distribution, and another normal distribution function to the G_2 + M peak. This computer code is a modified version of a generalized least-squares best-fit code written at LASL; the modification for the present purpose

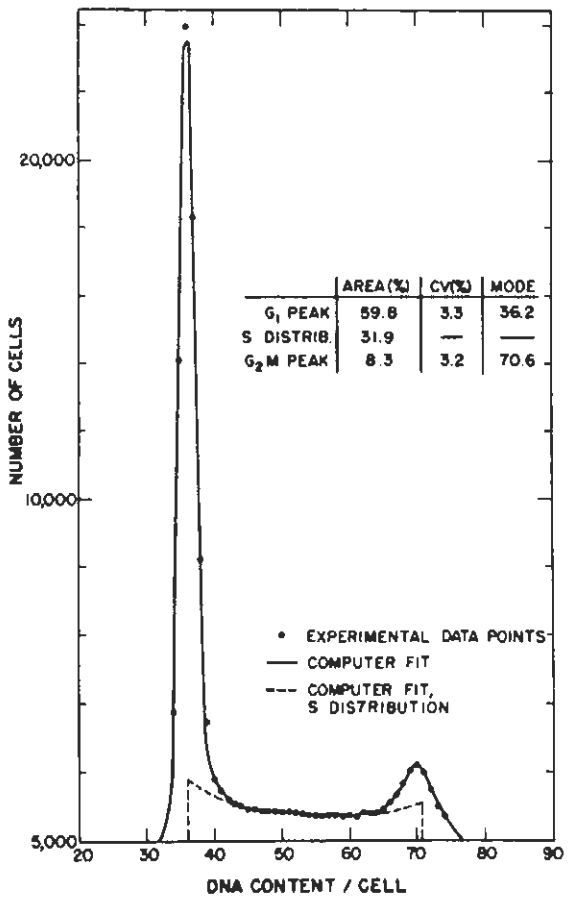

Fig. 1. Acriflavine-Feulgen-DNA distribution of suspension-cultured CHO cells, showing computer fit to the data and computer-generated output profile.

was made by P. N. Dean. Comparison of the areas under the G_1, S, and G_2 + M portions of the FMF distributions, determined by computer-fitting methods, is in approximate agreement with results obtained by biochemical cell-cycle analysis. This observation prompted the present study (namely, to compare quantitatively life-cycle analysis determined by FMF methodology with biochemical methods routinely used for life-cycle analysis). The FMF method offera the advantage of rapidly measuring very large numbers of cella, thus affording statistical precision hitherto unobtainable. Typically, 10^5 cells can be measured in a few minutes so that, in addition to precision, the experimenter has the combined advantage of a quantitative measure of each cell, short measuring time, and convenience.

A suspension culture of CHO cells seeded at low density and a set of monolayer culture flasks seeded simultaneously at low and equal cell density were sampled periodically as cells grew through the exponential to the stationary phase. A small aliquot of these cells was pulse-labeled with ^{3}H-thymidine (1 μCi/ml; Schwarz-Mann, 6 Ci/mM) for 15 minutes and processed for autoradiography. The remainder of cells in the sample were dispersed, fixed in formalin, and stored; all samples were stained by the acriflavine-Feulgen procedure as previously described (7) and measured by FMF on the same day. Feulgen-DNA distributions were analyzed by computer to obtain estimates of the G_1, S, and G_2 + M populations. The ^{3}H-labeled mitoses and total mitoses were scored from autoradiographic material to obtain the collection functions.

Results obtained from computer-fit analysis of Feulgen-DNA distributions obtained by FMF are shown in Table 1. Values of modal channel number and

TABLE 1. SEQUENTIAL CELL-CYCLE ANALYSES OF CHO CULTURES GROWING AS A SUSPENSION (S) OR AS REPLICATE MONOLAYERS[a]

Sample No.	G_1 Peak		G_2 + M Peak		G_2 + M Modal Channel / G_1 Modal Channel	Percent in G_1	Percent in S	Percent in G_2 + M
	Modal Channel	CV	Modal Channel	CV				
S1	34.3	3.67	68.0	3.83	1.98	44.4	48.6	6.5
S2	34.7	3.58	69.0	3.37	1.99	58.1	37.9	4.0
S3	35.0	3.58	69.0	3.78	1.97	58.2	37.1	4.71
M1	36.0	3.37	70.3	3.33	1.95	50.6	39.9	9.5
M2	34.8	3.19	68.3	3.38	1.96	45.2	45.4	9.4
M3	36.4	3.26	71.1	3.27	1.95	50.3	39.8	10.0
S4	31.3	3.94	62.3	3.83	1.99	61.5	33.1	5.4
S5	34.5	3.54	68.0	3.84	1.97	62.3	32.1	5.7
S6	35.6	3.64	70.0	3.95	1.97	66.1	31.0	2.9
S7	36.1	3.89	72.0	4.21	1.99	62.6	35.4	2.1
M5	35.1	3.44	68.6	3.49	1.95	52.7	36.5	10.8
M6	35.7	3.66	69.5	3.86	1.95	54.5	36.5	9.4
M7	36.2	3.26	70.6	3.60	1.95	60.2	36.1	7.6
All Data								
Mean	35.1	3.54	69.0	3.67	1.97			
SD[b]	1.27	0.223	2.26	0.275				
SE[c]	0.352	0.0618	0.627	0.0763				
All S Data								
Mean	34.5	3.69	68.3	3.83				
SD	1.43	0.147	2.77	0.231				
SE	0.540	0.0556	1.05	0.0873				
All M Data								
Mean	35.7	3.86	69.7	3.49				
SD	0.580	0.156	1.03	0.198				
SE	0.237	0.0637	0.420	0.0808				

[a] Samples at intervals of 2 to 4 hours were harvested and fixed. Data were computed by a least-squares best-fit code. Samples S1-2-3, M1-2-3 were stained and measured as one set and the remaining samples as another set 4 hours later.

[b] Standard deviation.

[c] Standard error.

coefficient of variation of the Gaussian functions which best fit the experimental peaks are shown. Channel number, as provided by the multichannel pulse-height analyzer, is proportional to cellular DNA content. These data cover changes in cell-cycle composition and also show a high degree of reproducibility: (a) the ratio of G_2 to M modal channel number to G_1 modal channel number is very close to 2.00, which is expected from genome duplication; (b) there is no statistically significant difference between modal channel number of the G_1 peak for suspension or monolayer cells, as expected; (c) because the mean channel number of the G_1 peak is 35.1, with a standard error of 0.352 channel (or 1 percent), the minimum detectable difference in cellular DNA content between two such populations measured with the same precision is $2\sqrt{0.352^2 + 0.352^2}$ or 1.00 channel (or 2.9 percent), suggesting the possibility of sex determination especially with haploid cells of favorable species such as humans; (d) the G_1 peak of the monolayer culture cells is slightly narrower than that for suspension culture cells, possibly due to a slight staining difference; (e) there is no statistically significant differeuce between the mean coefficients of variations of the G_1 and G_2 + M peaks, indicating certain instrumental dispersive effects (photon statistics, Raman scatter, and fluorescence) are negligible; and (f) standard error of the mean coefficient of variation of the G_2 + M peak is only slightly larger than the corresponding value for the G_1 peak. The fact that this difference is so small speaks well for the statistical precision of the data and validity of the computer analysis, as the G_2 + M peak not only is smaller than the G_1 peak but more obscured by the S-distribution.

The percentage of cells in S for monolayer and spinner cultures of CHO cells, as obtained from FMF data or ^{3}H-thymidine-labeled cell scoring, is presented in Table 2. Comparison of S values obtained by the two methods reveals, in most instances, that FMF data are in good agreement and are quite comparable to that obtained biochemically through pulse-labeling.

This study is still in the preliminary stages; however, these initial results have been quite promising, and it is felt that certain minor modifications in experimental design will minimize discrepancies that presently exist between results obtained by FMF and those obtained through biochemical methods.

TABLE 2. COMPARISON OF PERCENTAGE OF CELLS IN THE DNA-SYNTHETIC PERIOD (S) FOR MONOLAYER AND SPINNER CULTURES OBTAINED BY FMF AND RADIOACTIVE ^{3}H-THYMIDINE LABELING

Number	Fluorescent Microfluorometry	^{3}H-Thymidine Labeling
Spinner Culture		
1	48.6	40.6
2	37.9	34.8
3	37.1	35.4
4	33.1	33.2
5	32.1	29.4
6	31.0	26.6
7	35.4	25.0
8	28.4	20.6
9	25.3	31.4
10	27.6	25.0
11	25.6	21.0
Monolayer Culture		
1	39.9	37.0
2	45.4	40.2
3	39.8	36.0
4	a	37.0
5	36.5	29.6
6	36.1	41.6
7	32.3	30.8
8	24.7	27.2
9	9.5	9.2

[a]Sample tube broke during centrifugation, and FMF sample was lost.

REFERENCES

(1) *A. Howard and S. R. Pelc, Synthesis of Deoxyribonucleic Acid in Normal and Irradiated Cells and its Relation to Chromosomal Breakage, Heredity 6 (Suppl. 1):261-273 (1953).*

(2) *T. T. Puck and J. Steffen, Life Cycle Analysis of Mammalian Cells, Biophys. J. 3:379-397 (1963).*

(3) *C. P. Stanners and J. E. Till, DNA Synthesis in Individual L-Strain Mouse Cells, Biochim.*

Biophys. Acta 37:406-419 (1960).

(4) R. A. Tobey, D. F. Petersen, E. C. Anderson, and T. T. Puck, Life Cycle Analysis of Mammalian Cells, Biophys. J. 6:567-581 (1966).

(5) M. A. Van Dilla, T. T. Trujillo, P. F. Mullaney, and J. R. Coulter, Cell Microfluorometry: A Method for Rapid Fluorescence Measurement, Science 163:1213-1214 (1969).

(6) P. M. Kraemer, D. F. Petersen, and M. A. Van Dilla, DNA Constancy in Heteroploidy and the Stem Line Theory of Tumors, Science 174:714-717 (1971).

(7) P. M. Kraemer, L. L. Deaven, H. A. Crissman, and M. A. Van Dilla, The Paradox of DNA Constancy in Heteroploidy, In: Advances in Cell and Molecular Biology, Vol. 2 (E. J. DuPraw, ed.), Academic Press, Inc., New York, N. Y. (1972), in press.

(8) D. M. Holm and L. S. Cram, An Improved Instrument for Quantitative Cellular Fluorescence Measurements in Single Cells (in preparation).

Monitoring Ploidy of Cell Culture Systems by Flow Microfluorometry

Although cultured cell strains have many advantages over primary cell cultures for human virus vaccine production, several major questions relating to safety arise when one considers the use of such cells. One of these questions concerns chromosome constitution. Because cancer is usually accompanied by chromosomal changes, it appears prudent to require that such cell strains have the same karyology as normal primary diploid cells. Ploidy is generally considered as being an important parameter; therefore, ploidy monitoring of cell strains under development for vaccine production as a function of passage history is considered important by the Division of Biologics Standards of the National Institutes of Health, the agency responsible for promulgation of standards, licensing, and control of biologic products for human use. The possibility of using flow microfluorometry (FMF) for ploidy monitoring has been investigated through a mutual-interest conjoint AEC-NIH project. We have concluded that tetraploidy and heteroploidy can be detected with good sensitivity and accuracy. The question of aneuploidy (defined as near-diploid chromosome number) is still open because of the difficulty of obtaining such populations for combined cytogenetic and FMF study. Additional interest in aneuploidy has been generated by the finding of DNA constancy within heteroploid cell lines, which raises the question of whether aneuploid cell populations do, in fact, contain a cellular DNA content that differs from diploid cells and reflects chromosome number differences. This question is worth continued investigation.

The instrumentation and cell-dispersal and staining method for FMF has been described previously (1-5). Briefly, cells stained by a fluorescent Feulgen procedure flow at high speed, one-at-a-time, through a beam of intense blue light from an argon-ion laser. Resulting fluorescent light flashes are converted by a photomultiplier into analogous electrical pulses, which are analyzed and stored by a multichannel pulse-height analyzer. The resulting histogram reflects the DNA distribution of the cell population. Advantages of this are statistical precision, resolution, short measuring time, and convenience. Typically, 10^5 cells are measured in a few minutes; G_1 and G_2 + M peak coefficients of variation of 3.2 percent are obtained for some cell lines (HeLa, CHO) and 4 to 6 percent for a wide variety of other cell populations. Validation of the method to detect tetraploid, heteroploid, and small subpopulations with cellular DNA contents differing slightly (5 to 10 percent) from normal has been accomplished. Several fetal monkey cell strains currently under development by DBS (FRhL-2,3,4; FCL-1; FCK-3) have been monitored at a wide variety of stages in their passage history, and a small amount of tetraploidy seems to come and go intermittently and at random. A sudden rise, followed by a return to normal values, was observed occasionally. Data showing this type of behavior are shown in Tables 1 and 2 (see following page). Heteroploidy in these cell strains was not observed but could have been detected if present, as shown by experiments with the heteroploid rhesus line LLC-MK_2. Figure 1 shows the cellular DNA distributions for the heteroploid-diploid set for this species (see following page), and Table 3 lists quantitative DNA distribution and karyological data (see following page). As expected, the heteroploid population has considerable more DNA and chromosomes per cell than does the diploid

TABLE 1. SLIGHT, INTERMITTENT TETRAPLOIDY NORMALLY PRESENT IN STRAIN FRhL-3

Passage No.	Tetraploidy (percent, approximate)
16	ND*
18	ND
19	6
22	ND
23	ND
24	1-2
25	ND
26	ND
30	ND
32	1-2

*ND = none detected.

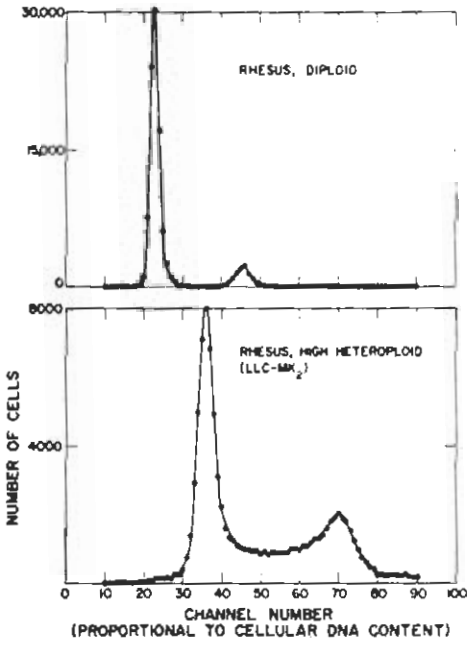

Fig. 1. Acriflavine-Feulgen-DNA distributions of rhesus monkey diploid (Rh) and high-heteroploid cultures.

TABLE 2. MONKEY CELL STRAINS RECEIVED FROM LEDERLE LABORATORIES (JUNE 1971)

Strain	Chromosome Data: Passage No.	Chromosome Data: Tetraploidy (percent)	FMF Data: Passage No.	FMF Data: Tetraploidy (percent)	FMF Data: G_1 Peak CV (percent)	Comments
FRhL-2	40	3	43	a few	9.4	
	50	29	51	35	8.9	
	60	50	64	a few	12.4	Considerable size variation, cytoplasmic fluorescence; cells look "cruddy"
	70	5	72	a few	9.0	
FRhL-4	45	11	48	a few	9.6	
FCK-3	5	--	8	--	-	Very slow growing; contaminated (not Rh) or aneuploid
	10	--	12	--	-	
	15	45	16	--	-	Slow growing; contaminated with Rh
	20	--	23	a few	8.5	

TABLE 3. COMPUTER-PROCESSED FMF ANALYSES OF GROWING CELLS AND CHROMOSOME NUMBER COUNTS OF METAPHASE CELLS OF VARIOUS MAMMALIAN CELL CULTURES

Species	Cell Type: Line	Karyotype	Channel	G_1 Peak[b]	G_2 + M Peak	Ratio: G_2 + M/G_1	G_1 Mode[a] Norm.	Chromosome Number: Number of Cells
Rhesus	Rh	Diploid	Mode	22.8	45.9	2.01	1.00	38 39 40 41 42 43 44 45 46 84
			Area	77.7	8.39			1 1 1 10 31 1 2 1 2 2
			CV	4.91	4.51	0.92		
	$LLC-MK_2$	High Heteroploid	Mode	35.7	72.2	2.02	1.57	56- 71- 132- 38 59 60 61 62 63 64 65 66 67 68 69 70 72 138
			Area	38.3	9.30			3 1 2 1 1 4 8 12 6 4 3 1 1 2 4
			CV	5.79	5.24	0.91		

[a]Diploid cells were considered to have a G_1 mode of 1.00; G_1 peak channel modes of other cells of the same species were normalized to this value.

[b]FMF gain was the same for all sets. Members of a species set were run within the same day. Day-to-day standardization varied slightly. Mode refers to channel number, while area and coefficient of variation (CV) are in percent.

population. Also as expected, the heteroploid population shows considerable chromosome number variability relative to the diploid population. However, dispersion of the G_1 and G_2 + M peaks is similar for both populations, as is the case for a wide variety of other heteroploid–diploid sets representing several species. This paradox of DNA constancy in heteroploidy is discussed elsewhere in this annual report; we merely point out here that heteroploid cell populations are distinctive by virtue of their cellular DNA content.

The problem of detection of aneuploidy (chromosome number = $2N \pm i$, where i = a few) has been investigated, yet an important question remains. Experiments with uniform fluorescent polystyrene microspheres as a nonbiological model system for a diploid cell population with an emerging subpopulation of cells of slightly different cellular DNA content have shown that such subpopulations are detectable if their abundance is 5 to 10 percent and cellular DNA content deviates from normal by 5 to 10 percent. Additional supporting data come from recent experiments using the colcemid reversal method (6) for inducing nondisjunctive errors in CHO cells. Because these mitotic errors produce a subpopulation with cellular DNA contents distributed about the normal value, the G_1 peak shape should be non-Gaussian. This was found to be the case, as shown in Fig. 2, where the base of the G_1 peak is broadened noticeably after 2 hours exposure to colcemid; the effect increases with exposure time. Taken together, these experiments show that aneuploidy, if reflected by a real deviation of cellular DNA content from normal, can be detected by FMF methods. The question of whether aneuploidy does, in fact, represent a real DNA deviation is still open and worthy of further investigation. We shall continue to be interested in making FMF measurements of aneuploid cell populations documented by standard cytogenetic methods; the larger the aneuploid subpopulation and its deviation from the diploid number, the better.

These observations on tetraploidy, heteroploidy, and aneuploidy are relevant to the question of the course of development of heteroploidy from a diploid strain as a function of passage history. There is evidence that this transition can take place by an increase in the tetraploid

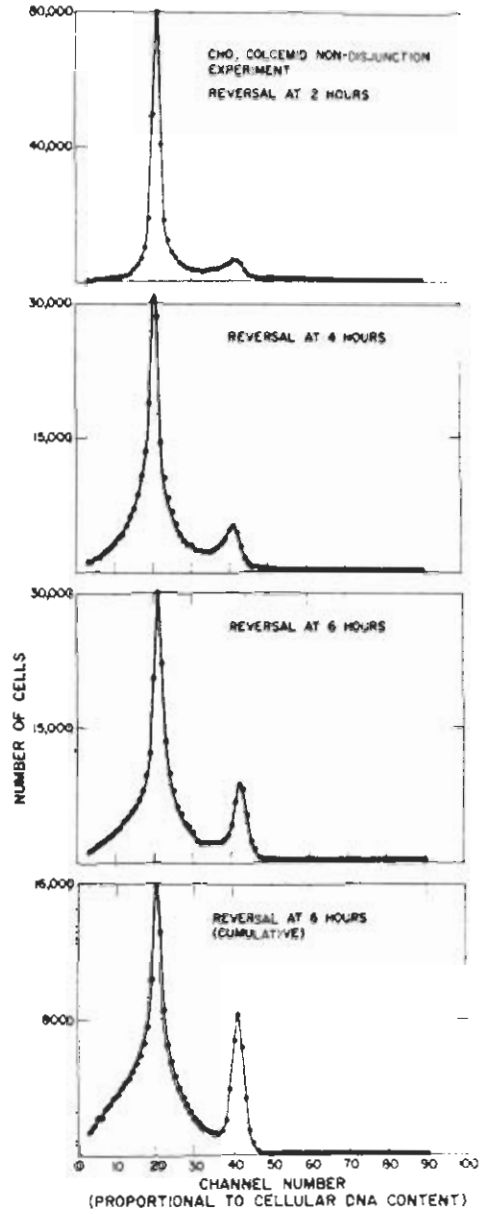

Fig. 2. Acriflavine-Feulgen-DNA distributions of CHO suspension cultures at various times after addition of 0.06 μg/ml colcemid. The residual G_1 peak at day 1 is at channel 20.7.

population, which is accompanied by a decrease and finally a disappearance of the diploid population and followed by some chromosomal loss resulting in a near-triploid population (7). Another possibility is that transition is related to small, gradual increases in chromosome number (i.e., aneuploidy). However, this mechanism requires accompanying increases in cellular DNA content;

therefore, investigation of this point seems worthwhile for the future if cell populations suitable for joint cytogenetic and flow microfluorometric study become available.

REFERENCES

(1) M. A. Van Dilla, T. T. Trujillo, P. F. Mullaney, and J. R. Coulter, Cell Microfluorometry: A Method for Rapid Fluorescence Measurement, Science 163:1213-1214 (1969).

(2) P. M. Kraemer, D. F. Peterson, and M. A. Van Dilla, DNA Constancy in Heteroploidy and the Stem Line Theory of Tumors, Science 174:714-717 (1971).

(3) T. T. Trujillo and M. A. Van Dilla, Application of the Fluorescent Feulgen Reaction to Cells in Suspension for Flow Microfluorometry, Acta Cytol. (1972), in press.

(4) D. M. Holm and L. S. Cram, An Improved Instrument for Quantitative Cellular Fluorescent Measurements in Single Cells (in preparation).

(5) P. M. Kraemer, L. L. Deaven, H. A. Crissman, and M. A. Van Dilla, The Paradox of DNA Constancy in Heteroploidy, In: Advances in Cell and Molecular Biology, Vol. 2 (E. J. DuPraw, ed.), Academic Press, Inc., New York, N. Y. (1972), in press.

(6) H. Kato and T. H. Yashida, Nondisjunction of Chromosomes in a Synchronized Cell Population Initiated by a Reversal of Colocemid Inhibition, Exp. Cell Res. 60:459-464 (1970).

(7) T. C. Hsu, Chromosomal Evolution in Cell Populations, In: International Review of Cytology, Vol. 12, Academic Press, Inc., New York, N. Y. (1961).

Immunofluorescent Measurements with Flow Microfluorometry

A cell-antigen system has been selected, characterized, and used successfully in experiments designed to demonstrate the value of flow microfluorometry (FMF) for quantitating immunofluorescent reactions. At the present time only the diffieult and tedious techniques of microspectrophotometry are available as an alternative method. The result has been a serious lack of good, quantitative data on statistically-significant numbers of cells. Among the problems of microspectrophotometry as applied to immunofluorescence are fading of the fluorescein isothiocyanate tag used to label the antigen or antibody, slow data accumulation, and insufficient illumination at the desired wavelengths of excitation. FMF was designed with these problems in mind, but its usefulness for measuring the weak fluorescence commonly associated with immunofluorescence had not been demonstrated. FMF offers the following advantages for quantitating immunofluorescence: (a) the fading problem is eliminated as each cell is in the exciting beam for only 3 μseconds; (b) the fluorescence of about 10^5 cells per minute can be measured; and (c) the exciting light is an argon-ion laser which has a very bright line at 488 nm to match the absorption maximum (490 nm) of fluorescein conjugates. Thus, high-speed FMF offers considerable potential value in identifying and characterizing immunofluorescent reactions. The purpose of this project was to investigate the feasibility of using FMF to detect virus-infected tissue culture cells treated with fluorescent antibodies. To accomplish this purpose, a routinely-used laboratory system was selected for which a fluorescent antibody serum neutralization test, as well as a direct virus assay, had been developed. Because Carbrey et al. (1) have completed extensive technique development for the routine diagnosis of hog cholera virus, it was selected as a model system. Hog cholera, an RNA virus, replicates in the cytoplasm of PK-15 cells. Infected cells reacted with hog cholera antibodies that have been tagged with a fluorescent molecule have a bright-green cytoplasm and a dark nucleus and can be detected by FMF.

The flow microfluorometer has been described in detail elsewhere (2). Minor optimizing modifications were made by changing the exciting wavelength to 488 nm, and a new Corning Model 3-69 barrier filter was installed for more efficient collection of emitted fluorescence. In addition, cell concentrations of infected and noninfected samples were monitored closely to ensure that equal numbers of cells were measured.

A characterization of the PK-15 cells was made. Primary swine kidney cells, well controlled PK-15 cell lines obtained from private investigators, and

PK-15 cell lines used routinely for virus assay were completed to determine which would be most suitable for virus assay by FMF. The DNA distribution of PK-15 cells used routinely for virus assay was measured with the FMF after staining the cellular DNA via the fluorescent-Feulgen reaction (3), as shown in Fig. 1. The DNA distribution was unique in that three peaks were found. The modal channel of each peak was separated in DNA content by a factor of two. Ruddle (4) has reported that PK-15 cell popnlations display the presence of more than one chromosome number (mixoploid); therefore, the DNA distribution was interpreted as consisting of a mixture of two cell populations, one of which contained exactly twice as much DNA as the other. This conclusion was confirmed by producing clones from single cells and measuring the resulting DNA distribution of the clones. Two clones are compared with the original cell population in Fig. 1. They are believed to be pure populations, as both clones have been through many passages to provide a sufficient number of cells (10^7) for FMF measurements.

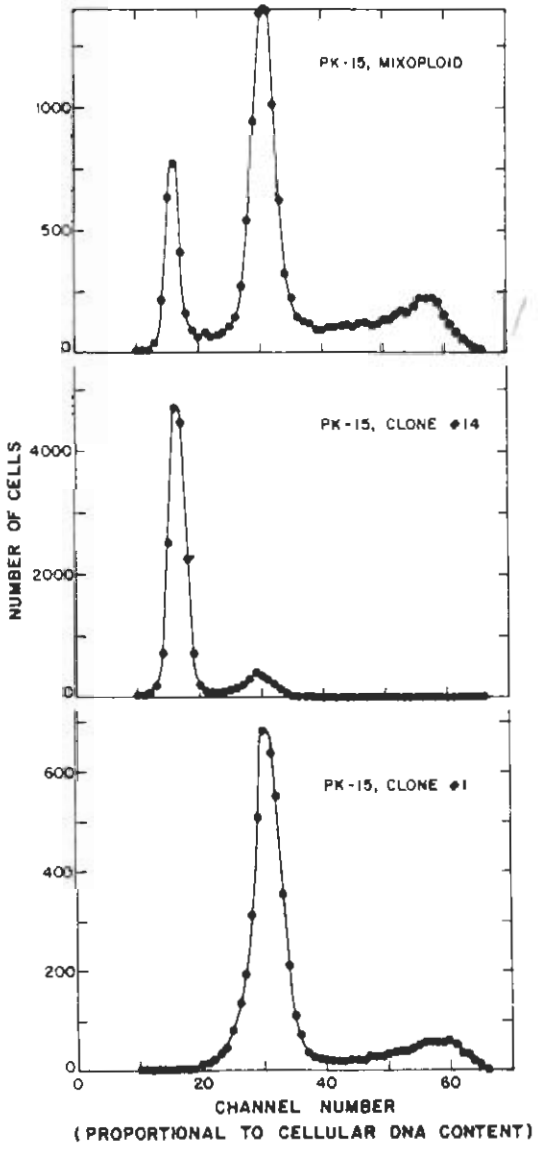

Fig. 1. Fluorescent-Feulgen-DNA distributions of PK-15 cells before and after cloning single cells.

Chromosome spreads from each clone were prepared by the squash technique. Initial chromosome counts indicated that the modal value of chromosome number distributions did not differ by a factor of two, as do the DNA distributions. Therefore, the PK-15 cell line is an ideal system for showing that DNA content is not necessarily proportional to chromosome number. This point is discussed in detail elsewhere in this annual report. Another interesting feature of this cell system that should make it a useful model system for studying cell differentiation is the fact that the cell populations are symbiotic. The fact that the two cell populations exist together without overtaking one another implies that their doubling times are equal or, more likely, that their generation times are not equal but that intercellular metabolic factors are being produced that differentially regulate cell doubling.

Using the clones illustrated in Fig. 1, we compared the rate of virus replication on diploid versus tetraploid PK-15 cells. Separate Leighton tubes were inoculated with the PK-15 cell clones and used in the assay for hog cholera virus. After treating the fixed monolayers with conjugate, the fluorescent plaques were compared for size and number. No significant differences were observed. This experiment will be repeated using FMF to quantitate the cellular fluorescence (i.e., number of intracellular antigens).

Techniques have been developed for preparing suitable cell suspensions and conjugate treatment of PK-15 cells that are compatible with requirements of FMF. Mechanical means of sample preparation which we investigated were found to damage the cells. The highest yield of intact cells in suspension was obtained by disperaing cell monolayers with trypsin and EDTA. Particular attention was given to the

development of a procedure that would allow single-cell suspensions to be fixed in cold acetone, as acetone is the fixative of choice for a large number of cell-antigen systems. To prevent cell clumping, extreme care must be exercised in handling the suspensions (done at 37°C). As a final step, cells are rinsed in phosphate-buffered saline to help remove nonspecific fluorescence.

The fluorescence distribution of maximally infected PK-15 cells reacted with conjugate and similarly treated but noninfected cells is illustrated in Fig. 2. This illustration demonstrates that FMF can distinguish the difference in fluorescence between populations of infected and noninfected cells. The technique also gives a means of estimating the amount of antigen in cells. The variation in cell fluorescence, much greater in infected cells as compared with control cells, was taken to indicate a great variation in viral antigen content between individual cells.

Preliminary serum-neutralization experiments have demonstrated that serum titers can also be measured by FMF techniques. Multiple antibody specificities in sera should also be measurable by FMF.

A few light-scatter studies have been made using a Science Spectrum Differential I light-scatter photometer that was available for a short time. The intensity of light scattered in the forward direction from viable, untreated suspensions of infected and noninfected PK-15 cells was compared. Maximally infected cells scattered approximately twice as much light at about 20° from the forward direction of the incident beam. The difference in scattering is most likely due to differences in internal structure of the cells, as has been predicted in theoretical calculations by Latimer (5). This is the first demonstration of such an effect for mammalian cells infected with viral antigens.

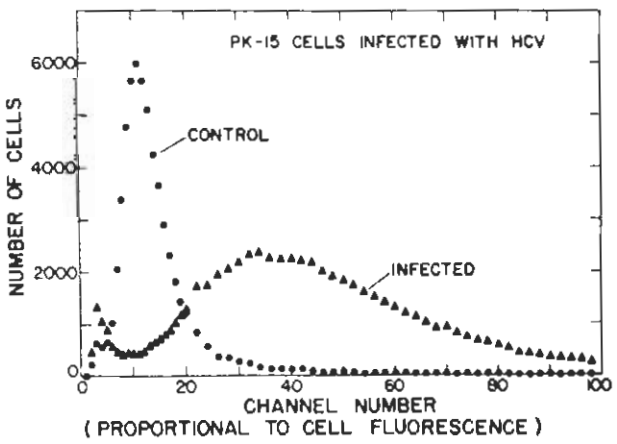

Fig. 2. Fluorescence distribution of PK-15 cells infected with hog cholera virus and noninfected PK-15 cells. Both samples were reacted with fluorescein labeled hog cholera antibodies.

We have demonstrated that flow microfluorometry can be used to distinguish the difference in fluorescence between infected and noninfected tissue culture cells. Techniques for preparing adequate samples of PK-15 cells infected with hog cholera virus have been developed. The general nature of the study should apply to other cellular immunofluorescent systems. Further optimization of preparative techniques and instrumentation, such as two-parameter analysis now under development, should produce even more clear-cut results.

REFERENCES

(1) E. A. Carbrey, W. C. Stewart, J. I. Kresse, and L. R. Lee, Confirmation of Hog Cholera Diagnosis by Rapid Serum-Neutralization Technique, J. Amer. Vet. Med. Assoc. 155:2201-2210 (1969).

(2) D. M. Holm and L. S. Cram, An Improved Instrument for Quantitative Cellular Fluorescent Measurements on Single Cells (in preparation).

(3) T. T. Trujillo and M. A. Van Dilla, Adaptation of the Fluorescent Feulgen Reaction to Cells in Suspension for Flow Microfluorometry, Acta Cytol. (1972), in press.

(4) F. H. Ruddle, Chromosome Variation in Cell Populations Derived from Pig Kidney, Cancer Res. 21:885-899 (1961).

(5) P. Latimer, D. M. Moore, and Q. Bryant, Changes in Total Light Scattering and Absorption Caused by Changes in Particle Conformation, J. Theor. Biol. 21:348-367 (1968).

(May 9-13, 1971), Abstract No. EC-12, pp. 55-56. Also in: Radiation Res. 47:287-288 (1971).

J. F. Spalding, L. M. Holland, and J. R. Prine, Studies of the Effects of Dose Protraction on Hematopoiesis in the Primate and Dog, In: Program/Abstracts of the 14th Plenary Meeting of COSPAR (Committee on Space Research), Seattle, Washington (June 17-July 2, 1971), Abstract No. L.3.2, p. 266.

J. F. Spalding, R. W. Freyman, and L. M. Holland, Effects of 800-MHz Electromagnetic Radiation on Body Weight, Activity, Hematopoiesis and Life Span in Mice, Health Phys. 20:421-424 (1971).

J. F. Spalding and L. M. Holland, Species Recovery from Radiation Injury, In: Survival of Food Crops and Livestock in the Event of Nuclear War, Brookhaven National Laboratory, Upton, New York (September 15-18, 1970), AEC Symposium Series 24:245-258 (December 1971).

J. F. Spalding and M. R. Brooks, The Possible Influence of a Single Gene Locus on Life Span and Its Relationship to Radiation Resistance and Activity, Proc. Soc. Exp. Biol. Med. 136:1031-1033 (1971).

Manuscripts Submitted

J. F. Spalding and M. R. Brooks, Longevity and Mortality Distributions of Mice with and without X-Ray Exposure to 45 Generations of Male Progenitors, Proc. Soc. Exp. Biol. Med. (in press).

J. F. Spalding, L. M. Holland, J. R. Prine, D. W. Farrer, and R. G. Brown, Effect of Continuous Gamma-Ray Exposure on Performance of Learned Tasks and Effect of Subsequent Fractionated Exposures on Blood-Forming Tissue, In: Proceedings of the National Symposium on Natural and Manmade Radiation in Space, Las Vegas, Nevada (March 2-5, 1971), NASA-SP document (in press).

MAMMALIAN METABOLISM SECTION

Publications

J. E. Furchner, C. R. Richmond, and G. A. Drake, Comparative Metabolism of Radionuclides in Mammals. V. Retention of Iridium-192 in the Mouse, Rat, Monkey and Dog, Health Phys. 20:375-382 (1971).

J. E. Furchner and G. A. Drake, Comparative Metabolism of Radionuclides in Mammals. VI. Retention of Niobium-95 in the Mouse, Rat, Monkey and Dog, Health Phys. 21:173-180 (1971).

J. E. Furchner, C. R. Richmond, and G. A. Drake, Comparative Metabolism of Radionuclides in Mammals. VII. Retention of Ruthenium-106 in the Mouse, Rat, Monkey and Dog, Health Phys. 21:355-365 (1971).

W. H. Langham, Plutonium Distribution as a Problem in Environmental Science, In: Proceedings of the Symposium on Distribution and Measurement of Plutonium in the Environment, Los Alamos, New Mexico (August 4-5, 1971), Los Alamos Scientific Laboratory Report LA-4756 (1971), pp. 3-11.

Manuscripts Submitted

J. E. Furchner, C. R. Richmond, and J. E. London, Comparative Metabolism of Radionuclides in Mammals. VIII. Retention of Beryllium-7 in the Mouse, Rat, Monkey and Dog, Health Phys. (submitted).

W. H. Langham and J. W. Healy, Maximum Permissible Body Burdens and Concentrations of Plutonium: Biological Basis and History of Development, In: Uranium, Plutonium and the Transplutonic Elements, Handbook of Experimental Pharmacology (J. H. Stannard, ed.), Springer-Verlag, Berlin-Heidelberg-New York (submitted).

W. H. Langham, Biological Implications of the Transuranium Elements for Man, In: Proceedings of the Eleventh Hanford Biology Symposium on the Biological Implications of the Transuranium Elements, Richland, Washington (September 26-29, 1971), Health Phys. (submitted).

BIOPHYSICS SECTION

Publications

L. J. Carr, R. D. Hiebert, W. D. Currie, and C. T. Gregg, A Stable, Sensitive, and Inexpensive Amplifier for Oxygen Electrode Studies, Anal. Biochem. 41:492-502 (1971).

L. J. Carr, J. H. Larkins, and C. T. Gregg, A Multi-Channel Recording Oxygen Electrode Amplifier

for Biochemical Studies, Anal. Biochem. 41:503-509 (1971).

L. S. Cram, Approaches to Prescreening, Acta Cytologica 15:265-266 (1971).

P. N. Dean and D. M. Holm, Pion Stopping Region Visualization Experiments, Radiation Res. 48:201-205 (1971).

M. J. Fulwyler, M. A. Van Dilla, and J. A. Steinkamp, Automated Cytology: An Integrated System of Cell Analysis and Sorting, In: Abstracts of the 4th International Congress of Cytology, London, England (May 23-27, 1971), Abstract No. 93, p. 100.

M. J. Fulwyler, Objectives of Automated Cell Analysis, Acta Cytologica 15:5-6 (1971).

M. J. Fulwyler, Prescreening: Electronic Sorting of Cells, Acta Cytologica 15:422-425 (1971).

M. J. Fulwyler, Sorting or Marking the Prescreened Cells -- Closing Remarks, Acta Cytologica 15:442-443 (1971).

D. M. Holm, Approaches to Prescreening, Acta Cytologica 15:267-269 (1971).

S. W. Jordan, P. N. Dean, and J. Ahlquist, Early Ultrastructural Effects of Ionizing Radiation, Am. J. Path. 62:35a (1971), Abstract No. 68.

P. F. Mullaney and J. A. Steinkamp, Other Parameter Descriptors to be Considered, Acta Cytologica 15:107-108 (1971).

P. F. Mullaney, T. T. Trujillo, and L. S. Cram, Preparation of Samples for Flow Photometers in Automated Cytology, Acta Cytologica 15:217-221 (1971).

P. F. Mullaney, L. S. Cram, and T. T. Trujillo, Closing Remarks on Sample Preparation, Acta Cytologica 15:233-234 (1971).

P. F. Mullaney, Approaches to Prescreening, Acta Cytologica 15:271-272 (1971).

P. F. Mullaney and J. R. Coulter, An Electronic Particle Counting and Dispensing Device for Use in Animal Injection Experiments, Rev. Sci. Instr. 42:1434-1436 (1971).

P. F. Mullaney and A. Brunsting, Detection and Identification of Mammalian Cells, In: Abstracts of the 162nd National Meeting of the American Chemical Society, Washington, D. C. (September 12-17, 1971), Abstract No. 13.

J. A. Steinkamp, M. J. Fulwyler, and J. R. Coulter, Electronic Cell Sorting by Volume, Light Scatter and Fluorescence, In: Proceedings of the 24th Annual Conference on Engineering in Medicine and Biology, Las Vegas, Nevada (October 31-November 4, 1971), Abstract No. 18A.7, p. 148.

M. W. Stewart, M. A. Van Dilla, and M. J. Fulwlyer, Requirements of Sample Collection and Preparation, Acta Cytologica 15:230-232 (1971).

M. A. Van Dilla and M. J. Fulwlyer, Cellular Parameters Measurable in Flow Systems, Acta Cytologica 15:98-102 (1971).

M. A. Van Dilla and M. J. Fulwyler, Other Parameter Descriptors to be Considered -- Closing Remarks, Acta Cytologica 15:115 (1971).

M. A. Van Dilla and T. T. Trujillo, Sorting or Marking Prescreened Cells, Acta Cytologica 15:441-442 (1971).

Manuscripts Submitted

A. Brunsting and P. F. Mullaney, Differential Light Scattering: A Possible Method of Mammalian Cell Identification, J. Colloid Interface Sci. (in press).

A. Brunsting and P. F. Mullaney, Light Scattering from Coated Spheres: A Model for Biological Cells, Appl. Optics (in press).

P. N. Dean, Summary of Session on Instrumentation Techniques, In: Proceedings of the Workshop on In Vivo Measurement of Heavy Elements, Lawrence Livermore Laboratory, University of California, Livermore, California (November 8-9, 1971), UCRL-report (submitted).

P. N. Dean, H. M. Ide, and W. H. Langham, External Measurement of Plutonium Lung Burdens, Health Phys. (submitted).

T. T. Trujillo and M. A. Van Dilla, Adaptation of the Fluorescent Feulgen Reaction to Cells in Suspension for Flow Microfluorometry, Acta Cytologica (in press).

ISOTOPE APPLICATIONS SECTION

Publication

C. T. Gregg and V. H. Kollman, The ICONS Program at LASL, In: Newsletter (New Mexico Institute of Mining and Technology), Socorro, New Mexico (1971), p. 7.

MAMMALIAN METABOLISM SECTION

W. H. Langham, Research, Past and Present, on Biological Effects of Point Source Radiation Exposure, presented at the Symposium on "Radiobiology, Past and Present," Argonne National Laboratory, Argonne, Illinois (April 2, 1971).

L. E. Agnew, B. J. Dropesky, W. H. Langham, H. A. O'Brien, and L. Rosen, The Los Alamos Meson Physics Facility (LAMPF): An Open Research Facility with Potentialities in Nuclear and Particle Physics, Biology and Medicine, Nuclear Chemistry, and Radionuclide Production, presented at the 47th Annual Meeting of the Southwestern and Rocky Mountain Division, American Association for the Advancement of Science, and the 15th Annual Meeting of the Arizona Academy of Science, Tempe, Arizona (April 21-24, 1971).

W. H. Langham, Electronic Sensing and Sorting of Normal and Abnormal Biological Cells, presented at the Science Writers Seminar, Argonne National Laboratory, Argonne, Illinois (May 24-25, 1971).

W. H. Langham, Plutonium Distribution as a Problem in Environmental Science, presented at the Symposium on "Distribution and Measurement of Plutonium in the Environment," Los Alamos, New Mexico (August 4-5, 1971).

W. H. Langham, General Aspects of the Plutonium Environmental Problem with Emphasis on Response to Inhaled Plutonium Particles, presented as a briefing lecture via telephone to Brooks Air Force Base, Texas (August 19, 1971).

W. H. Langham, Biomedical Applications of Negative Pions, presented at the Nuclear Medicine and Radiation Biology Laboratory, University of California, Los Angeles, California (September 21, 1971).

W. H. Langham, The Biological Implications of the Transuranium Elements for Man, presented at the 11th Hanford Biology Symposium on the Biological Implications of the Transuranium Elements, Battelle-Northwest, Richland, Washington (September 26-28, 1971).

W. H. Langham, Studies at Los Alamos of Employees with Long-Term Plutonium-239 Depositions, presented at a meeting of the U. S. Transuranium Registry, Battelle-Northwest, Richland, Washington (September 30-October 1, 1971).

W. H. Langham, Plutonium Distribution as a Problem in the Environment, presented at the Wichita Section Meeting, American Nuclear Society, Wichita, Kansas (October 13, 1971).

C. R. Richmond, Biological Studies Related to Radiation Exposure Standards, presented at the Desert Research Institute, Nevada Southern University, Las Vegas, Nevada (December 15, 1971).

BIOPHYSICS SECTION

A. Brunsting and P. F. Mullaney, Differential Light Scattering: A Possible Method of Mammalian Cell Identification, presented at the Symposium on the Occasion of the Centennial of Rayleigh Scattering Theory, American Chemical Society, Washington, D. C. (September 12-17, 1971).

L. S. Cram, Flow Microfluorometry: A Rapid Method of Determining DNA Distributions in Cell Populations, presented at the Department of Physics, Illinois Institute of Technology, Chicago, Illinois (January 27, 1971).

L. S. Cram, M. J. Fulwyler, and J. D. Perrings, Fluorescent Spheres for Cell Population Modeling in Automated Cell Analysis Systems, presented at the Annual Meeting of the Biophysical Society, New Orleans, Louisiana (February 16-18, 1971).

L. S. Cram, Flow Microfluorometry, A Rapid Method of Determining DNA Distributions in Cell Populations, presented at the University of Alabama, Birmingham, Alabama (February 22, 1971).

S. W. Jordan, P. N. Dean, and J. Ahlquist, Early Ultrastructural Effects of Ionizing Radiation, presented at the Annual Meeting of the American Association of Pathologists and Bacteriologists, Montreal, Quebec, Canada (March 6-9, 1971).

P. N. Dean, Instrumentation Techniques, presented at the Workshop on the In Vivo Measurement of Heavy Elements, Lawrence Livermore Laboratory, University of California, Livermore, California (November 8-9, 1971).

M. J. Fulwyler, Automated Cell Analysis in Cancer Prescreening, presented at the Science Writers Seminar, American Cancer Society, Carefree, Arizona (April 3-5, 1971).

M. J. Fulwyler, Automated Cell Analysis at the Los Alamos Scientific Laboratory, presented at

Coherent Radiation, Inc., Palo Alto, California (May 7, 1971).

M. J. Fulwyler, M. A. Van Dilla, and J. A. Steinkamp, Automated Cytology: An Integrated System of Cell Analysis and Sorting, presented at the 4th International Congress of Cytology, London, England (May 23-27, 1971).

P. F. Mullaney and J. R. Coulter, An Electronic (Coulter) Particle Counter for Use in Animal Injection Experiments, presented at the Annual Meeting of the Biophysical Society, New Orleans, Louisiana (February 16-18, 1971).

P. F. Mullaney and A. Brunsting, Detection and Identification of Mammalian Cells by Their Light-Scattering Properties, presented at the Symposium on the Occasion of the Centennial of Rayleigh Scattering Theory, American Chemical Society, Washington, D. C. (September 12-17, 1971).

P. F. Mullaney, Biophysics Research at the Los Alamos Scientific Laboratory, presented at the Sigma Xi Club lecture, University of Scranton, Scranton, Pennsylvania (September 17, 1971).

J. A. Steinkamp, Automated Cell Identification and Electronic Sorting, presented at the Department of Engineering Science, Florida State University, Tallahassee, Florida (January 13, 1971).

M. A. Van Dilla, P. N. Dean, and T. T. Trujillo, DNA Distribution of Cell Populations: Computer Analysis of Flow Microfluorometric Measurements, presented at the Annual Meeting of the Biophysical Society, New Orleans, Louisiana (February 16-18, 1971).

ISOTOPE APPLICATIONS SECTION

C. T. Gregg, Biological Applications of Carbon-13 at the Los Alamos Scientific Laboratory, presented at the First National Symposium on Carbon-13, Los Alamos, New Mexico (June 9-11, 1971).

C. T. Gregg, The ICCNS Program at LASL, presented at the 1971 New Mexico Branch Meeting, American Society for Microbiology, New Mexico Institute of Mining and Technology, Socorro, New Mexico (October 8-9, 1971).

C. T. Gregg, Nuclear Magnetic Resonance, presented at the Seminar on the Use of Stable Isotopes in Clinical Pharmacology, Center for Continuing Education, University of Chicago, Chicago, Illinois (November 10-11, 1971).

D. G. Ott, "Heavy" Mice, presented at the Science Writers Seminar, American Cancer Society, Carefree, Arizona (April 3-5, 1971).

D. G. Ott, Carbon-13 and Organic Chemistry, presented at the Chemistry Department, Utah State University, Logan, Utah (May 3, 1971).

D. G. Ott, Synthesis of Carbon-13 Compounds, presented at the First National Symposium on Carbon-13, Los Alamos, New Mexico (June 9-11, 1971).

D. G. Ott, Organic Synthesis and Biosynthesis, presented at the Seminar on the Use of Stable Isotopes in Clinical Pharmacology, Center for Continuing Education, University of Chicago, Chicago, Illinois (November 10-11, 1971).